Development of Carbon-Based Adsorbents for Phosphate Removal from Aqueous Solution

January 2020

He Hui

Development of Carbon-Based Adsorbents for Phosphate Removal from Aqueous Solution

A Dissertation Submitted to
the Graduate School of Life and Environmental Sciences,
the University of Tsukuba
in Partial Fulfillment of the Requirements
for the Degree of Doctor of Philosophy in Environmental Studies
(Doctoral Program in Sustainable Environmental Studies)

He Hui

Abstract

Phosphorous (P) is an essential nutrient and plays a critical role in the development of agriculture and industry. Phosphorus recovery from phosphate-rich wastewater has been recognized as a key strategy to prevent eutrophication and simultaneously solve the phosphorus shortage issue. Recently, carbon-based adsorbents are becoming increasingly attractive as they can be derived from a wide range of agricultural waste feedstocks and has been claimed to possess potentials as cost-effective, environmentally sustainable adsorbents for pollutants management. In this study, it is hypothesized that a low-cost adsorbent derived from agricultural waste (tobacco stalks) can remove excessive phosphate from aquatic systems effectively. Therefore, P can be retained in soils by reutilization of the spent composites as a slow-release fertilizer. The main results from the experiments can be summarized as follows.

Three novel iron-modified biochars were prepared through the pyrolysis of waste tobacco stalk and decorated by different modification (chemical co-precipitation of $FeCl_2$, $FeCl_3$ or Fe^{2+}/Fe^{3+} impregnation). The virgin biochar showed very limited phosphate removal amount of 0.49 mg P/g at an initial phosphate of 50 mg/L. In contrast, significantly improved phosphate sorption capacity was detected for the three novel biochars after ion modification. Freundlich model better fitted to the experimental data obtained from the three ion-modified biochars with higher R^2. The maximum adsorption capacities of $FeCl_2$-modified, Fe^{2+}/Fe^{3+}-modified biochar and $FeCl_3$-modified calculated from Langmuir equation were 7.24 mg/g, 7.50 mg/g and 17.4 mg/g, respectively. The pseudo n-order model ($R^2 > 0.96$) simulated the adsorption process better than the pseudo first-order and second-order model. The phosphate adsorption on $FeCl_3$-modified biochar was highly pH dependent and showed the highest phosphate adsorption ability (9.37 mg/g) at an initial pH of 2.52. The coexistence of sulfate, nitrate and chloride showed positively effect on phosphate adsorption onto the $FeCl_3$-modified biochar, while the presence of carbonate and bicarbonate could strongly compete with phosphate for the adsorption sites.

The MgAl-LDHs modified hydrochar composite was prepared through carbonization of tobacco stalks feedstock under hydrothermal conditions, serving as a sustainable supporting material that was modified simultaneously through a self-assembly synthesis of MgAl-LDHs to develop an effective and cost-efficient P removal adsorbent. Phosphate adsorption onto MgAl-LDHs modified hydrochar composite exhibited the largest capacity at initial pH 2, then the P adsorption amount decreased by only 2.08%-17.6% when the initial pH was increased from 4 to 8, while decreased rapidly when the initial pH was further increased to 12. The prepared composite possessed remarkably higher P adsorption capacity than the raw tobacco

stalk. Besides, phosphate adsorption could be completed within 1 h. The adsorption kinetic and isotherm data followed the pseudo-second-order equation and the Freundlich model (R^2 > 0.99), respectively. The maximum adsorption capacity calculated from the Langmuir model were 30.7, 31.4 and 41.2 mg P/ g at 25, 35 and 45 °C, respectively. The impact of other commonly coexisting anions on phosphate adsorption efficiency followed a descending order as carbonate > bicarbonate > sulfate > nitrate > chloride.

Finally, potential applications of $FeCl_3$-modified biochar and MgAl-LDHs modified hydrochar were evaluated, with the high content of NAIP and AP (> 93%) in TS-LDHs before and after adsorption. MgAl-LDHs modified hydrochar was comparatively recommended as a potential phosphatic fertilizer substitute. While, obvious enhancement of sludge dewaterability and P removal ability suggested $FeCl_3$-modified biochar could be a promising carbon-based composite for anaerobically digested sludge treatment.

Results from this work indicated that MgAl-LDHs modified hydrochar or $FeCl_3$-modified biochar composite could be a promising alternative of carbon-based adsorbent for phosphate removal from wastewater.

Keywords: Tobacco stalk; carbonization; modification; Phosphate adsorption; Wastewater

Contents

List of tables

List of figures

Abbreviations

AD	Anaerobically digested
AP	Apatite phosphorus
AWBs	Agricultural waste byproducts
BET	Brunauer-Emmett-Teller analysis
CST	Capillary suction time
EDS	Energy Dispersive Spectroscopy
FTIR	Fourier transform infrared
IP	Inorganic phosphorus
NAIP	Non-apatite inorganic phosphorus
OP	Organic phosphorus
P	Phosphorus
PAOs	phosphorus accumulating organisms
SEM	Scanning electron microscopy
TEM	Transmission electron micrograph
TS	Tobacco stalk
WWTPs	Wastewater treatment plants
XRD	X-ray diffraction

Chapter 1 Introduction

1.1 The world's phosphorus issue

Phosphorus (P) refers to an essential nutrient required by creatures in life circle, which ranks the second most abundant mineral (next to calcium) found in all plants and animals. Phosphorus, which plays a critical role in fundamental biochemical reactions, is billed as one of the basic composing elements of energy transfer and genetic material (Elser, 2012). Phosphorus is also a major player in phospholipids and the biomineral hydroxyapatite, functioning as a supporter of the structural membranes and bone of organisms (Reijnders, 2014).

However, Phosphorus, one of primary basic mineral nutrients for living species, is essentially nonrenewable and exhaustible mineral resource (Alatalo et al., 2013). Also, it is expected that P global reserves, which harbors the commercial feasibility will run out within 50-100 years. As a result of the sufficient food production needs of the growing population and the strong dependence on above 90% imports P was officially identified as one of the 20 critical raw materials in Europe (Krishnan and Haridas, 2008; Biswas et al., 2008). According to the 100 million Mg rock mine production in 2014, despite the fact that China still owes the 5.52% of the global total volume of P reserves (93.7 billion Megagrams), it may be depleted within 37 years, Furthermore, along with the world's population growth, P fertilizer will have be faced increasingly growing demand for food production and consequently its criticality. The last years have witnessed that intense discussion on these challenges about phosphorus shortage on scientific and various political levels (Elser, 2012; Lalley et al., 2016; Park et al., 2015).

1.1.1 Phosphorus as a pollutant (Water Eutrophication)

The exceedingly abundant existence of phosphorus within water systems, regarded for the reason of the accepted untreated wastewater from domestic, agricultural and industrial sources, helps promote eutrophication and uncontrolled algal blooms (Gao et al., 2017). Unfortunately, phosphate concentration was kept at low concentration of 0.02 mg/L , which gives rise to uncontrollable algae growth (Huang et al., 2017b; Lee et al., 2017). Algal blooms can limit light penetration, deplete dissolved inorganic carbon and oxygen content, release toxins, meanwhile enhancing pH to the extreme levels, thereby degrading growth and giving rise to die-offs of plants, fishes as well as aquatic wildlife, especially in the estuarine, shallow lakes, and the areas at coastal marine (Gnandi et al., 2006). Concerning the risk for causing the water body contamination and ecological unbalance, phosphorus demand is projected to

consolidate phosphate removal and subsequently (or simultaneously) recovery from wastewater, which is receiving high attention (Elser, 2012; Jung et al., 2015a; Liu et al., 2013).

1.1.2 Sources of aqueous phosphate

Discharge of high levels of phosphate into the aquatic ecosystems can accelerate eutrophication, thus causing the deterioration of the water quality. Additionally, aqueous phosphate's natural sources also constitutes a part of P natural circulation, including the decomposition of rocks, minerals and organism, sedimentation, storm water runoff, atmospheric deposition and so on (Anirudhan et al., 2006). As population growth and accelerated urbanization process, anthropogenic sources has become the principal source of the excess P in water bodies (Eljamal et al., 2013). Governing sources of aqueous phosphate's anthropogenic discharge come out of agricultural runoff, wastewater treatment facilities, and industrial wastewater, which contain high-level phosphate. Therefore, The P in discharges has increased to be the serious pollution sources as a response to constant growth in human behaviors. For instance, in the UK, up to 70% of overload phosphorus in water bodies are attributed to sewage discharges; agricultural run-off are another main source (European Commission, 2010). Another major participators to the growth in the concentrations of aqueous phosphate, agricultural production consumed about 40-million ton phosphorus fertilizers worldwide on a yearly basis (Hansen et al., 2017).

1.2 Control legislation of aqueous phosphate

Actively controlling the P contaminant in the sources of emissions and surface runoff can promote the effect efficient protection exerted by the aquatic ecosystems. The Australian Water Quality Guidelines, as a control measure, used for fresh and marine waters, has imposed a limited total phosphorus concentration within 0.010-0.100 mg/L range in rivers and streams; whilst the restriction for drinking water sources (reservoirs and lakes) is featured by more seriousness, which was 0.005-0.050 mg/L (Australian and New Zealand Environment and Conservation Council, 2000). The United States Environmental Protection Agency published the data that, rivers and streams had phosphorus contaminant level in Eco region criteria, fluctuating within the range of 0.010 to 0.076 mg/L. It is announced to be controling the reservoirs at less than 0.025 mg/L for the usage of drinking water (Neethling et al., 2011). In China, the effluents from wastewater treatment plants imposed a stringent phosphorus discharge standard limit of 1 mg/L (Ministry of Environmental Protection, China, 2002). Japan should have a variation between 0.005-0.100 mg/L in the pragmatic management targets for expected

phosphorus concentration in lakes and reservoirs (Ministry of the environment, 2003). UK has been involved in a general agreement that the volume of soluble reactive phosphorus emission to the water courses should be varying within the range of 0.100-0.020 mg/L, which depends on river type, with 0.2 mg/L as the interim for the rivers of heavy abundance (Environment Agency, 2000).

1.3 Current processes for phosphorus removal or recovery

Phosphorus removal technologies was originated at the beginning of the 1950s, aiming to degrade the levels of phosphorus in emissions and surface runoff and prevent the eutrophication. The technologies have attracted vastly growing research interest in the last few decades (Morse et al.,1998). Up to now, various methods have been available for controlling phosphorus, including precipitation, biological method, ion exchange, crystallization, tertiary filtration, adsorption, etc.

1.3.1 Precipitation

Initiated in Switzerland during the 1950s, chemical precipitation is a well-established practice to control the widespread growth of water eutrophication (Gutierrez et al., 2010). The main process of chemical precipitation is carried out with the additional divalent or trivalent metal salt which forms precipitates of insoluble phosphates. Then the sparingly soluble metal phosphates can be tackled by physical separation process, like sedimentation and filtration (Pratt et al., 2012). Magnesium (Mg^{2+}), aluminium (Al^{3+}), ferric iron (Fe^{3+}), ferrous iron (Fe^{2+}) and calcium (Ca^{2+}) are principle chemicals that have been put under most utilization for the removal of chemical phosphate, meanwhile suffering from the toughness within sludge disposal as well as effluent neutralization (Morse et al., 1998). The major elements for P precipitation are put in importance order of (1) P and precipitation agent's molar ratio, (2) ions concentration, (3) pH as well as (4) temperature. Hence, adequate phosphate concentration has to achieve thermodynamic super-saturation and precipitation, which occur spontaneously. Additionally, it has been evolved to less economically needed to attain the upgraded phosphate removal based on the chemical approach , aiming to suit the demands of phosphate discharge under the stringent regulations (Gutierrez et al., 2010; Liberti et al., 1979; Pratt et al., 2012).

1.3.2 Biological method

In the late 1950s, excessive phosphorus was reported to have more than normal biomass growth requirement, which could be exploited by activated sludge under suitable conditions (Lu and Liu, 2010). Based on these research, biological approaches such as increased biological phosphorus removal, assimilation, constructed wetlands, wastewater stabilization pond and other influential aspects, were developed for phosphorus removal from waste water (Pratt et al., 2012). It has to be composed into phosphorus accumulating organisms (PAOs) for biological phosphorus removal to carry out the considerable excess phosphorus. Besides, they shall be addressed and then taken away from the system in the form of sludge. During the growth PAOs, they are not only consuming phosphorus for cellular components, but also accumulating large quantities of polyphosphate in their cells (Yuan et al., 2012). The technology is advantageous in the application of chemicals by excessing sludge production. Nonetheless, this process is featured by high varieties as a result of operational challenges with less trace-level efficiency, which results from the reality that insufficient phosphate degrades microorganisms metabolism (Yuan et al., 2012). More importantly, special care and strict control are inclined to be demanded while biological method was being carried out (Huang et al., 2017a; Lalley et al., 2016).

1.3.3 Ion exchange

The exchange of undesirable ions was made for solid-phase ion affinity in the process billed as ion exchange (Crittenden et al., 2005). In comparison with other technologies, ion exchange offers a more optional approach to separating ions from solution, which has lately received recognition in P-removal applications (Muhammad et al., 2019). Ion exchange is seen as a hopeful approach for P recovery as a reversible process in general (Kuzawa et al., 2006). Moreover, the concentrated ionic solution is advised for the recovery of P in virtue of the treatments like calcium hydroxide precipitation with $CaCl_2$ addition. It is reported that a lot of promising ion-exchange processes have been made for P removal and recovery, such as capacitive deionization on oppositely charged electrodes, metal-loaded chelating resin and hydrotalcites (Rittmann et al., 2011).

1.3.4 Crystallization

The 1970s witnessed the start of crystallization technology for the removal of phosphorus out of waste water, which was involved in a direct precipitation and development of a crystal based on the induction of the seeding materials (Zoltek, 1974; Kim et al., 2006). A

crystallization process could be composed of three steps: supersaturation formation, nucleation (crystal birth) and crystal growth (Donnert et al., 1999). During two major crystallization processes, phosphate could be removed in virtue of the generation of calcium phosphate (Ca-P) or struvite ($MgNH_4PO_4{\cdot}6H_2O$) on the surface of seed crystals. The presentation on principal chemical reaction for the crystallization of phosphate in calcium phosphate or struvite is given as follows (Song et al., 2006; Peng et al., 2018):

$$5Ca^{2+} + 3PO_4^{3-} + OH^- = Ca_5(PO_4)_3OH \quad (1\text{-}1)$$

$$Ca^{2+} + HPO_4^{2-} = CaHPO_4 \quad (1\text{-}2)$$

$$3Ca^{2+} + 2PO_4^{2-} = Ca_3(PO_4)_2 \quad (1\text{-}3)$$

$$Mg^{2+} + H_nPO_4^{n-3} + NH_4^+ + 6H_2O = MgNH_4PO_4 \cdot 6H_2O + nH^+ \quad (1\text{-}4)$$

Where n=0, 1, 2, etc., which related to the solution pH.

Several researches have demonstrated the applicability of calcium phosphate and struvite achieved recovery from the crystallization reactor system and then recycled as a phosphorus resource (eg. slow-release fertilizer). Compared to the precipitation based on Fe and Al salts or lime for phosphorus removal, crystallization is able to achieve more stringent phosphorus removal requirements by creating a more marketable commercial product. Basic investigations contributed to possible applications are based on both municipal waste waters of low phosphorus concentrations, in addition to industrial effluents with remarkably higher phosphorus contents, which is in the volume of 400 mg/L (Peng et al., 2018; Kim et al., 2006).

1.3.5 Tertiary filtration

The growth of tertiary filtration begun in the 1900s, responding to polish effluent, phosphorus removal occurred by accident. The recovered sludge arising out of backwashing lacks for recycling suitability (Morse et al., 1998). However, tertiary filtration processes is designedly renowned for their capability of removing phosphorus. Up to now, various commercial filters products have been developed, such as slow sand filters, shallow bed filters and rapid gravity filters, rapid deep-bed filters and moving bed filters as well as pressure filters (Altmann et al., 2015; Morse et al., 1998).

1.3.6 Adsorption

Adsorption is involved in the transfer and accumulation of inorganic P from liquid-phase solutes to the surface of reactive solid-phase adsorbents (Brix et al., 2001). Of all the numerous phosphorus removal technologies, adsorption process has been recognized as a comparative economy and effective approach. Nevertheless, the adsorption process can decrease phosphate

concentration during the discharge for a much lower level, compared to the chemical approach. The growth of adsorbents with superior adsorption and regeneration ability can further upgrade phosphate removal and minimize sludge disposal, thus ultimately achieving the adsorption cost-effective oriented with practical application (Lalley et al., 2016; Li et al., 2016c). Besides, the adsorption could be applied for both phosphate removal, and phosphate recovery. To date, a wide variety of materials e.g. aluminium and iron oxides (Borggaard et al., 2005), calcite (Karageorgiou et al., 2007), fly ash (Lu et al., 2009), rice husk as well as fruit juice residues (Yadav et al., 2015), engineered biochar (Vikrant et al., 2018), activated carbon (Kumar et al., 2010) and others have been selected as adsorbents for phosphate removal from wastewater. Although the development of multiple natural or man-made materials have sped up and promoted the potential for the application of adsorptive phosphate remediation technologies, there have arisen a series of open questions and challenges, which require further detailed investigations within this field. The efforts to the performances of phosphate adsorption mainly concentrate on the following aspects: simple and easy synthesis methods, low costs, higher removal efficiencies and easy regeneration capabilities (Li et al., 2016a). Recently, taking into consideration the intensified "green thinking" in industry and the designated requirements, the treatment in virtue of the abundant and low-priced natural by-products to water/wastewater has been evolved to be a practical choice. The eco-friendly alternatives to expensive adsorbents, which include industrial by-products/wastes, residues from agriculture, soils, constituents, clay minerals and others, have been put to intensive the application (Huang et al., 2017b; Mohan et al., 2014).

1.4 Development of agricultural waste based phosphate adsorbents

1.4.1 Potentials of agricultural waste for phosphorus removal

Agricultural waste byproducts (AWBs) are characterized by several attributes which constitute for their attraction as the substrate to develop phosphorus biosorbents. First of all, AWBs are easily available, low-cost, and eco-friendly. In addition, AWBs is made up of large number of functional groups (e.g. -OH, -CHO) in their celluloses, hemicelluloses and lignin components. Hence, AWBs can be correlated to chemical reactions. That offers a fundamental principle for AWBs for the convert to be some functional polymers. Particularly, the -OH group of AWBs could integrate alkoxyamine ligands, thus improving their anion exchange capabilities (Biswas et al., 2008). It is likely that the application of AWBs phosphate biosorbents will bring about some profits. First, this application is able to defend the surface

water from being eutrophicated. Next, there will be a large volume of AWBs which are turned out all over the world on a yearly basis, which is imposing a challenge on the solid waste treatment. Therefore, not only do the AWBs recycling as phosphate adsorbents provide a viable solution in order to make waste materials economically in an eco-friendly mode, it but also provides additional vales for AWBs (Jung et al., 2015a; Mohan et al., 2014). It is suitable for the slogan of ‘‘use of renewable resources” stuck by Green Chemistry. Moreover, the exertion of adsorbents which is derived from abundant, cheap and renewable AWBs, might be helpful to the expense of phosphorus remediation. Furthermore, by shifting phosphorus in wastewaters to fertilizers, the commitment is able to make revenues. Also, successful wastewaters-based phosphorus exploitation will cut down the application mineral phosphorus, which, accordingly and undoubtedly saved the global phosphorus rock resource (Park et al., 2015). Evidently, phosphate adsorbents the based on a wide variety of AWBs is likely offer a sustainably effective and rewarding resolution to phosphorus pollution control.

1.4.2 Agricultural waste modification for improved phosphorus removal

An increasingly growing trend has been applied to AWBs, which is employed as phosphate biosorbents (Karthikeyan et al., 2002). Nonetheless, a lot of pristine AWBs is almost impossible to take away any phosphorus out of aqueous solutions, other methods take on low sorption abilities, in comparison with commercial adsorbents (Table 1-1). Phosphate removal of original AWBs expressed in the lacking efficiency is interpreted by rich by negatively charged functional groups (e.g. -OH, -COOH); in the meanwhile the positively absence charged the functional groups (e.g. -NH_2) on raw AWBs’ surface (Jack et al., 2019; Qiu and Duan, 2019). Thereby, AWBs has to be put under modification, in order to enhance their phosphate affinity. Additionally, AWBs modification was established to strengthen the merits of lignocelluloses materials. Hence, mitigating the organic matters release into aqueous solutions. Metal loading and thermal activation represents the two methods which are most widely-spread and some researches related on the focus are listed in Table 1-2.

1.5 Objectives and originalities

The main aim of this research is to develop innovative, cost-effective and sustainable carbon-based adsorbents derived from agricultural waste (tobacco stalks) for phosphate removal and evaluate its potential applications. This multipurpose technology will not only contribute to phosphate-rich wastewater management, but also be propitious to maintain agricultural sustainability. The originalities of this research can be represented as follow:

i. Tobacco stalks, a typical agricultural waste, were firstly used as carbonization biomass feedstock to develop low-cost and effective phosphate adsorbent.

ii. Functionalized hydrochar posing effective phosphate removal capability were developed through one-step hydrothermal preparation, which is rarely reported in previous research, and could be an innovative approach for abundant agricultural organic solid wastes utilization.

iii. Evaluation the potential of P-loaded carbon-based adsorbents as phosphatic fertilizer, in which P can be retained in soils and having positive effects on the restoration of soil ecosystem and carbon sequestration.

iv. Carbon-based adsorbents were firstly employed for wastewater sludge treatment as an attempt for simultaneously phosphorus removal and sludge conditioning.

1.6 The contents and framework of this research

The research could be divided into five parts, which were presented chapter by chapter and summarized as below:

The first chapter, firstly stated the world's phosphorus issue about the water eutrophication and shortage of phosphorus as well as the control policies of aqueous phosphate. Secondly, detailed summary was made on the current technologies for phosphorus removal/recovery. Thirdly, illustration was made on potentials of agricultural waste for phosphate adsorbents development. Further, some review was conducted on the literatures related to metal loading and thermal modification of agricultural waste for enhanced phosphate removal. The final section was the presentations on the objective, originalities and framework of this study.

In the second chapter, three novel iron-modified biochars derived from waste tobacco stalk were prepared through the pyrolysis combined impregnation way. Phosphate sorption capacities of the three iron-modified biochars were compared by isotherm studies. Batch adsorption experiments were conducted to study the influences of various conditions, like contact time, initial pH and co-existing anions on phosphate removal. The iron-modified biochars were also characterized in order to analyzing the implied mechanisms.

In the third chapter, the MgAl-LDHs modified hydrochar composite was prepared through carbonization of tobacco stalk feedstock in solution under hydrothermal conditions. The phosphate removal efficiency with varying parameters of environmental conditions, including initial solution pH, adsorbent dosage, contact time, temperature and the initial concentration of phosphate were evaluated. The relational coefficients of kinetics and isotherms were investigated and the adsorption mechanisms involved were also discussed in detail.

In the fourth chapter, two aspects of potential application routes of synthesized composite were studied. One was about the potential of P-loaded carbon-based adsorbents as phosphatic fertilizer, another was pertaining to the synthesized carbon-based composite employed for digested sludge treatment.

In the last chapter, according to the results of above three chapters, the main conclusions of this research were summarized and future research aspects were pointed out.

The experimental scheme was illustrated in Figure 1-1.

Table 1-1. The maximum phosphate adsorption capacity of commercial and natural AWBs based adsorbents.

Adsorbent	q_m (mg P /g)	Ref.
Giant reed	0.27	Xu et al. (2011)
Sugarcane bagasse	0.36	Zhang et al. (2016)
Coir pith	1.42	Krishnan and Haridas (2008)
Palm surface fibers	4.35	Ismail (2012)

Table 1-2. Comparison of different technologies for carbon-based P adsorbents development.

	Pyrolytic method	Pyrolytic conditions	Modification agents	Modifier quantity	The key of materials	characteristics	q_m (mg P/g)	Ref.
Cotton stalks	Pyrolysis	350 (-)	$FeCl_3$, NaOH	-	Ferric oxides dispersed on the inner and external of biochar granule	The surface areas and pore volumes increased effectively	0.96	Ren et al. (2015)
Sugarcane harvest residue	Pyrolysis	550 (1 h)	$MgCl{\cdot}6H_2O$, $FeCl_3$, NaOH	20wt %	Formation of the iron and magnesium oxides	Produce more pores and higher surface area	121.25	Li et al. (2016c)
water hyacinth	Pyrolysis	450 (1 h)	$FeCl_3$ and $FeCl_2$ (1:1 M ratio)	1:15 w/v	Inmobilization of Fe_3O_4 and Fe_2O_3	A predominance of 65.9% (atomic ratio) Fe and O of the total surficial elements	5.13	Cai et al. (2017)
soybean straw	Pyrolysis	500 (2 h)	$MgCl_2$ (190.42 g/L) and $AlCl_3$ (266.66 g/L)	1:7 w/v	Mg/Al oxides and oxyhydroxides flakes	The abundance of oxygen-containing functional groups and high surface areas	24.30	Yin et al. (2018b)
Rice straw	HTC	200 (10 h)	$LaCl_3$, KOH	30 wt %	A synergistic effect of hydrochar and lanthanum in P removal	Lanthanum might be in amorphous form	61.57	Dai et al., (2014)

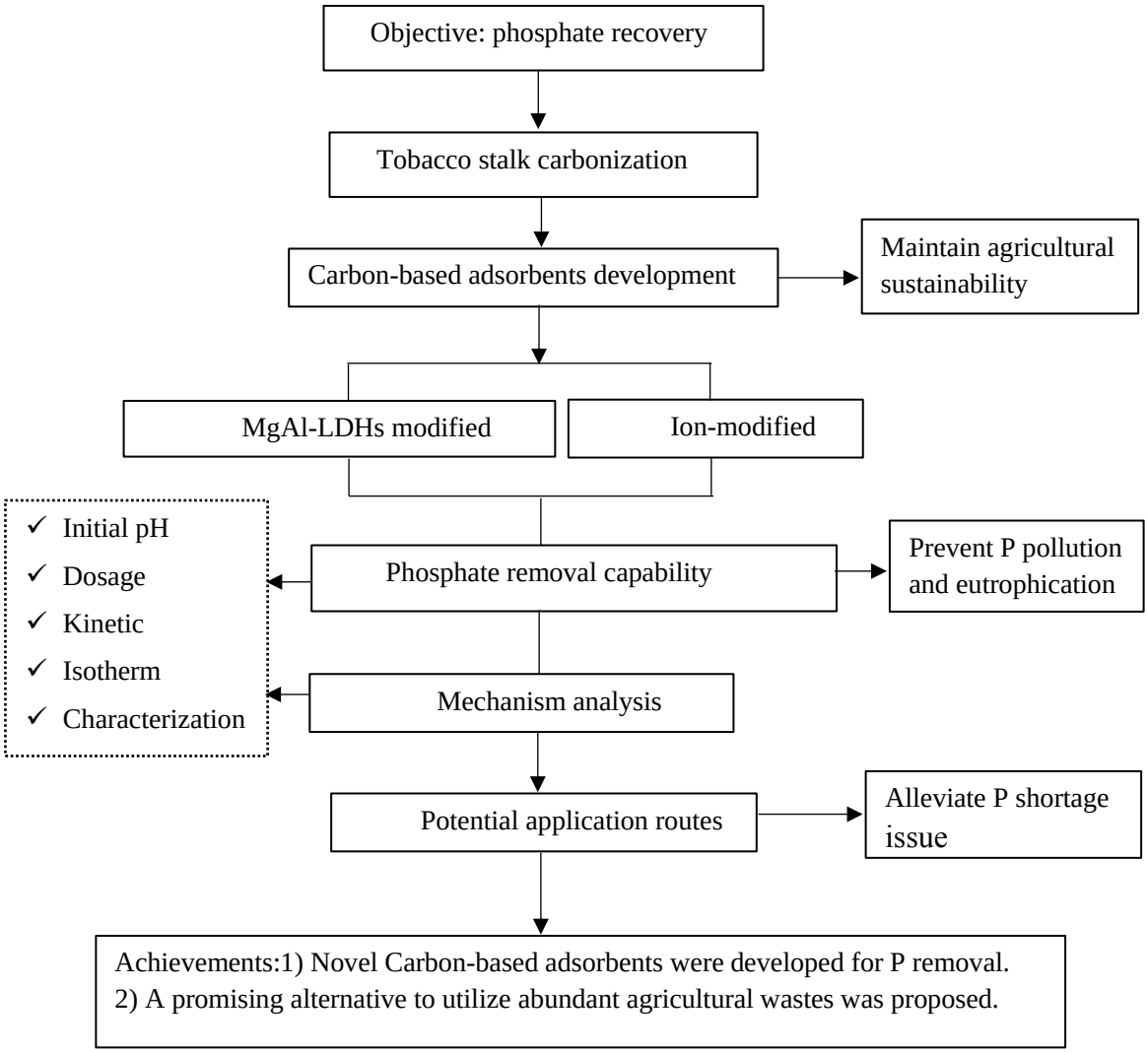

Figure 1-1. Overview of the experimental framework of this thesis.

Chapter 2 Efficient phosphate removal from wastewater by iron-modified biochars derived from tobacco stalk

2.1 Background

Biochar, a porous carbonaceous solid products derived from pyrolysis (>250 ℃) of biomass under oxygen-limited conditions, has received increasing attention in agronomic and environmental applications (Jung et al., 2016). As it's featured by superior performance in resisting decomposition and mineralization, biochar could be an effective way for long-term carbon sequestration (Cowie et al., 2015). When applied to the environment, biochar can remediate water pollution, enhance soil fertility and mitigate of global warming (Case et al., 2014; Wei et al., 2018).

Recent years have seen the excellence that biochar is being focused on as a latent adsorbent under the treatment of underwater as a result of the porous structure as well as rich functional groups, and environment-friendly features like low cost, various sources (Cha et al., 2016). A number of studies have demonstrated that biochar is of particular effectiveness to remove such organic compounds as polychlorinated biphenyls, dye, naphthalene and antibiotics (Chen et al., 2011; Cha et al., 2016). Moreover, biochar harbors a great deal of adsorption capacity to satisfy various heavy metals such as Pb, Cd, Cr, Cu and Zn (Park et al., 2016). Nonetheless, the raw biochar harbors phosphate adsorption capacity which is relatively low for the reason that it has restrained functional groups based on negatively charged surfaces (Jack et al., 2019; Yin et al., 2018a). Obtained biochar, for example, comes from crops displayed the phosphate adsorption capacity of low degree (< 0.3 mg P/g) (Takaya et al., 2016). Hence, raw biochar's modification is routinely used to enhance its affinity towards phosphate.

In terms of improving biochar properties for phosphate removal, according to prior researches, decorating biochar binding with metal oxides or hydroxides is able to enhance its adsorption performance oriented with phosphate in a large scale with employed iron modification. In comparison with other modified approaches the activation from sulfuric acid and lanthanum, for example, iron modification is characterized by simple and efficient features. The iron modified approach is billed as is an efficiently resource-saving strategy which is capable of improving the phosphate adsorption on biochar. Ren et al. (2015) conducted exploration on the phosphate adsorption capacity from cotton stalk biochar with the modification of granulation and chemical precipitation made by ferric oxides. Chen et al. (2011)

conducted investigation on the phosphate adsorption properties of orange peel biochar from the decoration of co-precipitation of Fe^{2+}/Fe^{3+} on alkaline condition in air as well as following pyrolyzation under the circumstances of different temperatures. However, few researches pay attention to the different effects of valence condition of iron in biochar modification.

In addition, on a yearly basis, large amounts of produced agricultural waste by-products have imposed a severe issue from the perspective of specific economy and environment. For example, Tobacco, a typical economic crop, is widely planted all over the world and could generates a huge amount of stalk biomass annually (1,000 kg ha^{-1}), causing environmental burden (Li et al., 2008; Xia et al., 2012). Therefore, it is important to explore effective utilization approach of agricultural solid waste in a green way. Tobacco stalk, as biomass feedstock for biochar matrix based phosphate adsorbent development, poses dominant advantages, such as easy acquiring, abundant availability and low cost. Furthermore, phosphorous contained in tobacco stalk biomass could be recovered, as well as the abundant phosphate in wastewater. However, the preparation of functionalized biochar derived from tobacco stalks and its utilization on P removal have not been reported and also needs to research.

The present work aims to fabricate three novel iron-modified biochars through the pyrolysis of waste TS and decorated by different modification (chemical co-precipitation of $FeCl_2$, $FeCl_3$ or Fe^{2+}/Fe^{3+} impregnation), and then evaluate the capabilities for P recovery from aqueous solution. To be specific, the physicochemical properties of the resultant biochars composite were characterized by X-ray diffraction (XRD) analysis, Fourier transform infrared (FTIR) spectroscopy, Brunauer-Emmett-Teller analysis (BET), and scanning electron microscopy (SEM). Adsorption kinetics, adsorption isotherms, and the effects of various operation conditions on phosphate adsorption were examined in details. The adsorption mechanism was also discussed.

2.2 Materials and methods

2.2.1 Chemicals and materials

Tobacco stalk (TS) were collected as the feedstock of biochar from a local farm in Yunnan province of southwest China. The TS was washed, dried, and then chopped and grinded, finally sieved through 80 meshes before use.

Analytical grade Ferric chloride hexahydrate ($FeCl_3 \cdot 6H_2O$), Ferrous chloride tetrahydrate ($FeCl_2 \cdot 4H_2O$), sodium hydroxide (NaOH), hydrochloric acid and monopotassium phosphate (KH_2PO_4) were purchased from Wako Pure Chemical Industries Ltd., Japan and used without

further purification. All experimental solutions were prepared using deionized water (DW), which was also used to rinse and clean the samples.

2.2.2 Preparation of biochars

The iron-modified biochars were obtainted through a pyrolysis and impregnation combined process. Dried TS powders were filled into a porcelain crucible whithout extra space left, then covered by tinfoil with some little holes and porcelain cap for pyrolyzing. The crucible was placed into a muffle furnace, the temperature was raised to 550°C with a heating rate of 5°C/min, and the temperature was maintained at 550°C for 2 h .After the furnace cooled down, the biochars were collected, washed to remove impurities, oven dried at 105°C and crushed to fine particle.

Three different iron-modified biochars were prepared by adding 3 g TS pristine biochar powder into 90 mL solution containing 0.3 mol/L Fe^{2+}/ $Fe^{3+}$of corresponding solution. Under vigorous magnetic stirring, 1 mol/L NaOH solution was added dropwise into the above suspension until the pH value reached 11. The resulting mixture kept stirring for 45 min followed by aged over night whithout stirring. The separated solid was washed, dried in oven, ground and stored in airtight containers. The obtained biochars were denoted as based on the immobilization solution as folllow: Biochars decorated by co-precipitation of solution containing 0.3 mol/L $FeCl_2$ or $FeCl_3$ denoted as TS-Fe(Ⅱ) or TS-Fe(Ⅲ), respectively; Biochar decorated by impregnation with the mixture of both 45 mL containing 0.3 mol/L $FeCl_2$ and $FeCl_3$ labelled as TS-Fe(Ⅱ/Ⅲ).

2.2.3 Characterizations of biochars

The morphology features of the samples were characterized by a field emission gun scanning electron microscopy (FEG-SEM, Nova NanoSEM 450). The Fourier transform infrared (FTIR) spectra were recorded using a Thermo Fisher model Nicolet iS5 in ATR mode. Surface areas of pure biochars and ion-modified biochars samples were measured with a Quantachrome Uadrasorb-evo surface area analyzer using the N_2 (BET) adsorption methods. The pH value was determined by a pH meter. Bruker AXS Inc D8 ADVANCE was used for taking the powder XRD patterns to determine the crystallographic structure of the samples.

2.2.4 Phosphate adsorption experiments

Batch adsorption experiments were conducted to investigate the performance of three novel biochars as phosphate removal adsorbents. All the batch adsorption samples were shaken

at 120 rpm and room temperature. After specific adsorption time, all the mixtures were filtered through 0.45 μm membrane filter and phosphate concentrations in the supernatants were measured by the standard methods (4500-P E) (APHA, 2012). The amount of phosphate adsorbed per unit mass of adsorbent q_e (mg/g) was calculated by the following equation:

$$q_e = (C_i - C_e) \times V/m \quad (2\text{-}1)$$

where V is the solution volume (L), C_i and C_e is the initial and equilibrium phosphate concentrations (mg/L), and m is the mass of the adsorbent (g), respectively.

All the experimental treatments were performed in duplicate and the average values are reported. Additional analyses were conducted whenever two measurements showed a difference larger than 5%.

(1) Phosphate adsorption isotherm

To examine the adsorption isotherm of the three novel ion-modified biochars, 0.1 g sample was added into 20 mL phosphate solutions with different initial concentrations ranging from 5 to 800 mg P/L. After 24 h, the adsorption capacity at equilibrium was calculated and the experimental data were described by the Langmuir and Freundlich models (Jung et al., 2016) as shown in the following equations:.

Langmuir isotherm model: $q_e = \frac{q_m K_L C_e}{1+K_L C_e}$ (2-2)

Freundlich isotherm model: $q_e = K_F C_e^{1/n}$ (2-3)

where q_e is the adsorbed amount of phosphate per unit weight of adsorbent (mg/g) at an equilibrium concentration of adsorbate in solution (C_e, mg/L). K_L and K_F are the Langmuir and Freundlich constants, respectively. q_m denotes the maximum adsorption capacity and n is the heterogeneity factor.

(2) Phosphate adsorption kinetics

Adsorption kinetics of phosphate on three ion-modified biochar samples were conducted by mixing 1 g adsorbent and 200 mL of 50 mg/L phosphate solution. At appropriate time intervals, the supernatant was taken and filtered to measure the phosphate concentration. The kinetic data were fitted to the pseudo-first-order, pseudo-second-order and pseudo-n-order (general order) kinetic models. The respective expressions of the three models are presented as follow (Yao et al., 2011; Tan et al., 2017; Riahi et al., 2017):

pseudo-first-order： $q_t = q_e \times (1 - e^{-k_{p1}t})$ (2-4)

pseudo-second-order： $q_t = \frac{k_{p2} q_e^2 t}{1+k_{p2} q_e t}$ (2-5)

pseudo-n-order: $q_t = q_e - \frac{q_e}{[k_{Pn}(q_e)^{n-1}\times(n-1)+1]^{1/1-n}}$ (2-6)

where K_{P1} and K_{P2} represent the rate constants for the pseudo-first-order model (min^{-1}) and pseudo-second-order model [g/(mg min)], respectively. q_t and q_e are the uptake amount of P for per unit adsorbent weight at a certain time *t* and at equilibrium (mg/g), respectively. K_{Pn} is the general order constant rate, n is the order of kinetic adsorption (n could be an integral or a fractional number).

(3) Effect of solution pH and coexisting anions

The effect of initial solution pH on phosphate adsorption was investigated by mixing 0.1g adsorbent and 20 mL of 50 mg/L phosphate solution at desirable pH values from 2.5 to 11.5. To study the influence of coexisting anion, each 20 mL of 50 mg/L phosphate solution containing 0.0016 M or 0.016 M NaCl, $NaNO_3$, $NaHCO_3$, Na_2SO_4, Na_2CO_3 solution was mixed with 0.1 g sample to determine the phosphate adsorption performance of biochars.

2.3 Results and discussion

2.3.1 Characterization of modified biochars

XRD analyses is employed to characterize the crystalline structure of iron modified biochars and the XRD patterns is shown in Fig. 2-1. TS-Fe(Ⅱ) and TS-Fe(Ⅱ/Ⅲ) samples presented the similar distribution of peak position. The strong diffraction peaks at 30.2°, 35.7°, 43.4°, 57.3°, and 63.1° were coincident with the phase of maghemite (Υ-Fe_2O_3) as the major crystalline in TS-Fe(Ⅱ) and TS-Fe(Ⅱ/Ⅲ) samples (Qiu et al., 2019; Wang et al., 2019). Peaks were keen-edged at 53.8° indicating the presence of Fe_3O_4 (He et al., 2018). There are no obvious characteristic peaks observed in TS-Fe(Ⅲ), indicating the sample existed in amorphous nature (Zhou et al., 2013).

The FTIR spectra of the three novel ion-modified biochars before and after P adsorption are shown in Fig. 2-2. The results mainly showed differences on the wavenumber interval of 2000-500 cm^{-1}. The band around 1561 cm^{-1} and 1352 cm^{-1} corresponds to asymmetric stretching of C=O in carboxylic groups and amine group, respectively. After P adsorption, the peak centered at 627 cm^{-1} and the strong peak at 553 cm^{-1} assigned to Fe–O of iron oxide (Zhu et al., 2018), were nearly disappeared; the intensity of peaks at 875 and 800 cm^{-1} attributed to the Fe–OH vibrations were reduced (Qiu and Duan, 2019). Meanwhile, the bands initially at 1049 cm^{-1} could be attributed to the phosphate groups (Huang et al., 2020), because P commonly exists in the raw biomass. After phosphate adsorption, the typical characteristic peak of the asymmetric

stretch vibration of P–O shifted to broader absorption peak at 1033 cm^{-1}. The results suggesting the interaction between ion oxygen groups and P species with possible formation of inner-sphere complexation via ligand exchange (Liu et al., 2018).

2.3.2 Adsorption isotherms

The adsorption isotherms were conducted to investigate the phosphate adsorption capacity of three ion-modified biochar samples. The fitted isotherms and the corresponding parameters are summarized in Fig. 2-3 and Table 2-2, respectively. The virgin biochar, produced by pyrolyzing TS at 550 °C without any modification, showed very limited phosphate removal amount of 0.49 mg P/g at initial phosphate of 50 mg/L. In contrast, significantly improved phosphate sorption capacity was observed with three novel biochars after ion modification with an order of TS-Fe(Ⅲ)> TS-Fe(Ⅱ/Ⅲ)> TS-Fe(Ⅱ). Freundlich model provides a better fitness than Langmuir model for phosphate adsorption on all three ion-modified biochars with higher R^2, indicating a multilayer process of phosphate adsorption onto the ion-modified biochars (Chen et al., 2017). The maximum adsorption capacity of TS-Fe(Ⅱ), TS-Fe(Ⅱ/Ⅲ) and TS-Fe(Ⅲ) calculated by Langmuir equation were 7.24 mg/g, 7.50 mg/g and 17.4 mg/g, respectively. Thus, TS-Fe(Ⅲ) was selected for the further adsorption experiments. Besides, it is noticed that when TS-Fe(Ⅲ) was applied into low concentration phosphate (5 mg/L) solution, the phosphate removal efficiency could exceed 98%, exhibited its feasibility to reclaim low concentration phosphate from contaminated water. In addition, three novel biochars synthesized in this study showed higher phosphate adsorption capacity compared with some other iron-impregnated biochars (Table 2-4).

2.3.3 Adsorption kinetics

The effect of contact time on phosphate adsorption onto TS-Fe(Ⅲ) was carried out and the results were showed in Fig. 2-4. TS-Fe(Ⅲ) exhibited a rapid phosphate adsorption in the first 90 min, to be specific, 87% of the ultimate adsorption completed within the first 10 min and up to 96% ultimate adsorption occurred until 90 min. After that, followed by an extremely sluggish adsorption stage until equilibrium was reached in 5 h. In order to clarify the mechanism involved, the experimental data were fitted to pseudo first-order model pseudo, second-order model and pseudo n model pseudo, the corresponding parameters are summarized in Table 2-3. According to the correlation coefficients, the pseudo n model (R^2 > 0.96) simulated the process better than the pseudo first-order and second-order model, implying that the reaction

order *n* determined by the experiment was 3.26, and phosphate adsorption on TS-Fe(Ⅲ) might be controlled by multiplex process (Tan et al., 2017; Ribas et al., 2014). The result was consistent with other ion-modified adsorbent on phosphate adsorption (Cai et al., 2017).

2.3.4 Effects of pH on phosphate removal

The phosphate adsorption capacities of TS-Fe(Ⅲ) and the final solution pH value after adsorption within the initial pH range 2.52–11.17 were shown in Fig. 2-5. The results shown that, the amount of phosphate adsorbed decreased with increasing of pH value. In particular, the amount of adsorbed phosphate was 9.37 mg/g at pH 2.52 and reduced to 3.61 mg/g at pH 11.17. The pH value of actual wastewater generally ranged from 6.0 to 8.0, at which TS-Fe(Ⅲ) showed middle level of adsorption capacity. Notably, with initial pH increasing from 2.52 to 9.01, the final solution pH value increased with reducing increments to the range of 6.52-9.87. Slightly decline of final pH to 10.01 and 10.68 were observed when the initial solution pH further increased to 10.34 and 11.17, respectively.

The significant effect of pH on phosphate adsorption, mostly due to the pH-dependent phosphorus speciation and the surface property of the TS-Fe(Ⅲ). Theoretically, when pH is between 2 to 12, $H_2PO_4^-$ and HPO_4^{2-} were the dominant species form of P in solution (Wang et al., 2019). At lower pH, the OH^- groups at the surface of TS-Fe(Ⅲ) were protonated ($-OH_2^+$), which may easily adsorb the negatively charged phosphorus species ($H_2PO_4^-$ and HPO_4^{2-}) via electrostatic attraction (Shi et al., 2019; Wang et al., 2018). Moreover, the adsorption free energy of HPO_4^{2-} was considerably higher than that of the $H_2PO_4^-$, and HPO_4^{2-} was the primary specie at lower pH (2.15–7.20) (Jack et al., 2019). Therefore, $H_2PO_4^-$ was easier attracted to the adsorption site on biochar surfaces and lower pH was beneficial for the adsorption on TS-Fe(Ⅲ). When pH further increased, the surface of TS-Fe(Ⅲ) was deprotonated, the electrostatic repulsion between negative phosphorus species and negatively charged surface sites, as well as the OH^- compete for adsorption active sites bring about the decline of phosphate adsorption.

In addition, the equilibrium pH after phosphate adsorption was 8 to 10 with initial solution pH at 4 to 10, which is likely related to the protonation or deprotonation of surface hydroxyl groups as well as the concentration of OH^-.

2.3.5 Effects of coexisting anions on phosphate removal

Coexistent anions are commonly distributed in actual wastewater wastewaters and may potentially interfere with phosphate for the binding sites (Qiu and Duan, 2019). The influences of several common coexisting anions, including Cl^-, SO_4^{2-}, NO_3^-, CO_3^{2-}, HCO_3^- on the phosphate removal capability of TS-Fe(Ⅲ) were showed in Fig. 2-6. The P adsorption capacities were slightly increased with the presence of 0.0016 M SO_4^{2-}, Cl^- and NO_3^- respectively, and further increased by 13.37%, 10.94% and 8.21% with the coexistent of higher concentration of these anions (0.016 M SO_4^{2-}, Cl^- and NO_3^- respectively). However, in the presence of 0.0016 M CO_3^{2-} and HCO_3^- reduced the adsorption amount of phosphate by 8.82% and 27.96% respectively, and further reduced by 14.89% and 42.55% with the concentration of CO_3^{2-} and HCO_3^- increased to 0.016 M. Generally, phosphate has also been considered to form inner- sphere complexes with metal hydroxides through specific adsorption, while Cl^-, SO_4^{2-} and NO_3^- often was weakly bound with surface sites forming outer-sphere complexes, which led to the ineffective competition on phosphate removal. Notably, the addition of coexisting anions could influence the solution pH, which plays a critical role on phosphate adsorption as illustrated in section 3.4. Thus, the final pH of the solution after adsorption process were detected and the results showed that the coexistent of CO_3^{2-} and HCO_3^- bring the pH to high levels greatly and further exhibited the most prominent inhibition on phosphate adsorption. In order to eliminate the effect of solution pH, extra experiments were conducted by adjusting the pH to the level when no addition of CO_3^{2-} and HCO_3^- ions. It is clearly showed in Fig. 2-6 that the phosphate removal ability with the presence of CO_3^{2-} and HCO_3^- obviously increased with initial pH decreased. In specific, adsorption amount of phosphate increased by 17.02% and 14.59% with the presence of 0.0016 M and 0.016M CO_3^{2-} respectively. While, in the case of HCO_3^-, adsorption amount of phosphate showed no obvious difference with control group. It therefore appears that the adverse effect of CO_3^{2-} and HCO_3^- ascribed principally to the buffering effects on pH value rather than the competition of bonding sites with phosphate species. Besides, both the induced decline of pH value and the increase of ionic strength contributed to the slight increase in phosphate removal capability. Overall, TS-Fe(Ⅲ) possesses a high selectivity toward phosphate, and the results also emphasized adjusting pH to acidic side was more favorable for phosphate capture onto TS-Fe(Ⅲ) in practical wastewater treatment.

2.3.6 Adsorption mechanism

According to the above results and analysis, the main mechanism of this study may be clarified as follow: during Fe^{2+}/ Fe^{3+} chemical co-precipitation process, the surface and channels of the pyrolyzed TS biochar were occupied by Fe^{2+}/ Fe^{3+} ions, which then become hydroxylated with the addition of NaOH, thus ion (hydr)oxide decoration improving the surface property and increasing the active sites of TS biochar. As shown in the BET analysis (Table 2-1), $FeCl_3$ modified biochar possessed the largest specific surface area, which were favorable for the adsorption and mass transfer of phosphate species, contributing to the comparatively higher phosphate removal capability (Lalley et al., 2016; Wang et al., 2016). Fe^{2+} was unstable and easily oxidized under an oxygen free atmosphere, the principle reaction during the Fe^{2+}/ Fe^{3+} chemical co-precipitation process can be illustrated as following:

$$Fe^{2+} + 2Fe^{3+} + 8OH^{-} \rightarrow Fe_3O_4 + 2H_2O \quad (2\text{-}7)$$

$$2Fe(OH)_2 + 1/2\, O_2 + H_2O \rightarrow 2Fe(OH)_3 \quad (2\text{-}8)$$

$$2Fe(OH)_2 + 1/2\, O_2 \rightarrow Fe_2O_3 + 2H_2O \quad (2\text{-}9)$$

The equilibrium pH after phosphate adsorption was increased to 8-10 with initial solution pH ranged from 4 to 10, and the pH increments was increased with the increasing of phosphate removal capability, indicating OH^- group was released to the solution during the adsorption process. In addition, Fe–O of iron oxide were nearly disappeared and the Fe–OH vibrations were reduced after phosphate adsorption onto three iron-modified biochars, while vibration related to P–O shifted to broader absorption peak at 1033 cm^{-1}. The observation suggesting the interaction between ion oxygen groups and P species with possible formation of inner-sphere complexation via ligand exchange, and the main reaction could be presented as follow:

$$TS - Fe - OH + H_2PO_4^- + H^+ \rightarrow IMB3 - Fe(H_2PO_4) + H_2O \quad (2\text{-}10)$$

Based on the above, the adsorption of phosphate onto three novel ion (hydr)oxide decorated biochar should be primarily attributed to the formation of Fe-P compounds via ligand exchange. Meanwhile, as illustrated in section 2.3.4, electrostatic attraction between negatively charged phosphate species ($H_2PO_4^-$ and HPO_4^{2-}) and electropositive adsorbent surface could also be involved in the adsorption process.

2.4 Summary

In this work, three novel iron-modified biochars were prepared through the pyrolysis of waste TS and decorated by different modification. Significantly improved phosphate sorption

capacity was detected for the three novel biochars after ion modification. The maximum adsorption capacities of $FeCl_2$-modified, Fe^{2+}/Fe^{3+}-modified and $FeCl_3$-modified biochar calculated from Langmuir equation were 7.24 mg/g, 7.5 mg/g and 17.43 mg/g, respectively. Freundlich model and pseudo second-order model better fitted to the experimental data obtained from the three ion-modified biochars with higher R^2. $FeCl_3$-modified biochar exhibited a rapid and acid favorable phosphate removal, and the existence of other anions, like sulfate, nitrate, chloride carbonate and bicarbonate could hardly compete with phosphate species. The main mechanism involved should be proposed as ligand exchange and electrostatic attraction. In general, $FeCl_3$-modified biochar, with low-cost, good selectivity, and high adsorption capacity, could be an attractive adsorbent for phosphorus-rich wastewater remediation.

Table 2-1. Summary of BET analysis results of iron modified biochars.

Adsorbents	BET surface area (m^2/g)	Pore volume (cm^3/g)	Average pore diameter (nm)
Raw biochar	3.97	-	-
TS-Fe(Ⅱ)	134	2.21	6.62
TS-Fe(Ⅱ/Ⅲ)	132	2.34	7.08
TS-Fe(Ⅲ)	232	2.44	4.19

Table 2-2. Freundlich and Langmuir constants and correlation coefficients for phosphate adsorption onto iron modified biochars.

Adsorbent	Langmuir			Freundlich		
	K_L (L/mg)	q_m (mg/g)	R^2	K_F (mg/g)/(mg/L)^n	n	R^2
TS-Fe(Ⅱ)	0.01	7.24	0.871	0.55	2.55	0.975
TS-Fe(Ⅱ/Ⅲ)	0.126	7.50	0.855	2.21	4.72	0.968
TS-Fe(Ⅲ)	0.031	17.43	0.864	3.07	3.39	0.985

Table 2-3. Kinetic parameters of phosphate adsorption onto TS-Fe(Ⅲ) (initial P concentration=50 mg P/L, adsorbent dosage=5 g/L).

Pseudo-first-order			Pseudo-second-order			Pseudo-n-order		
K_{p_1} (1/min)	q_e (mg/g)	R^2	K_{p_2} [g/(mg min)]	q_e (mg/g)	R^2	K_{p_n} [1/min $(g/mg)^{n-1}$]	q_e (mg/g)	R^2
0.366	6.6	0.584	0.136	6.771	0.903	0.045	7.030	0.963

Table 2-4. Comparison of phosphate adsorption capacity with other iron-impregnated biochars.

Feedstock	Pyrolysis (°C; h)	Modification	Adsorption condition (°C; pH)	Dosage (g/L)	C_i (mg/L)	q_m (mg/g)	Ref.
Corn cobs Garden wood waste Wood chips	500;2	Fe^{3+}	24 ± 2; –	33.3	10–200	1.99 2.75 3.20	Micháleková-Richveisová et al. (2017)
Orange peel	250;6 400;6 700;6	Fe^{2+}/Fe^{3+}	–	–	0-12	0.219 0.512 1.24	Chen et al. (2011)
Fly ash Coal gangue	500;1	Fe^{3+}	24.9;6	12	10-50	3.08 3.20	Qiu et al. (2019)
Tobacco stalk	550;2	Fe^{2+} Fe^{2+}/Fe^{3+} Fe^{3+}	25;-	5	5-800	7.24 7.50 17.4	This study

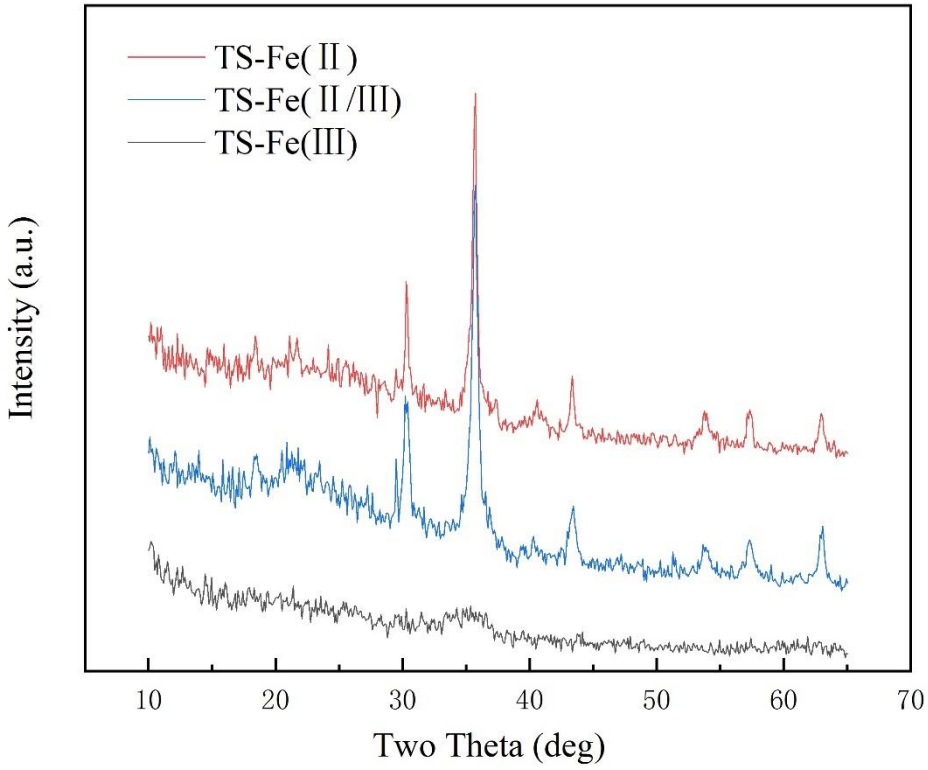

Figure 2-1. XRD patterns of three novel biochars.

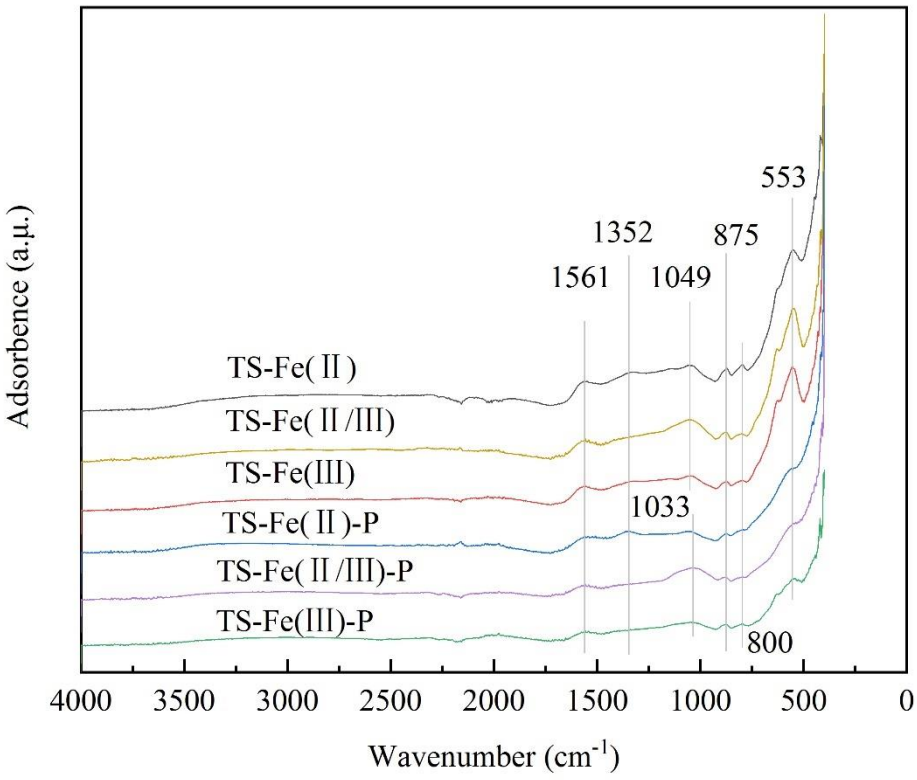

Figure 2-2. FTIR spectra of biochars before and after adsorption of phosphate.

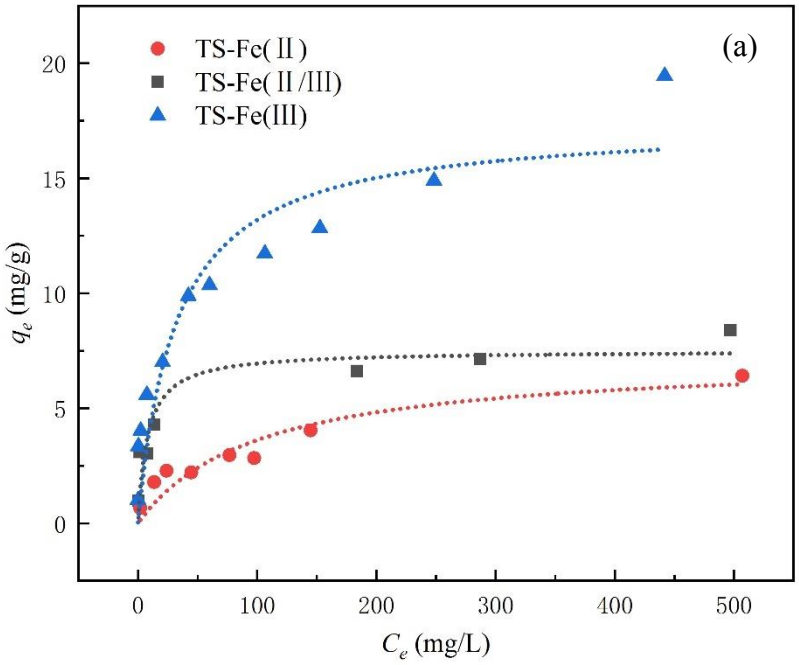

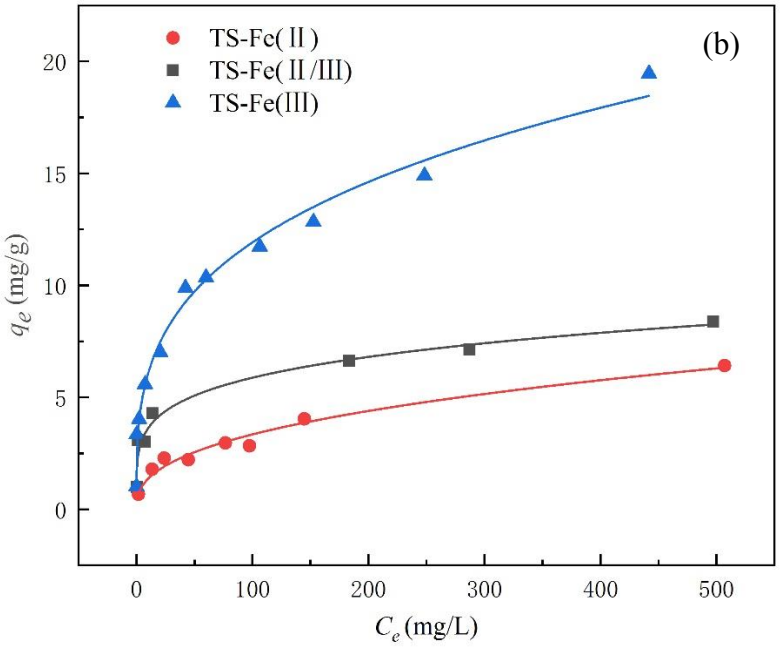

Figure 2-3. Adsorption isotherms of phosphate onto iron modified biochar Langmuir (a) and Freundlich (b) (initial P concentration=5-500 mg P/L, adsorbent dosage=5 g/L).

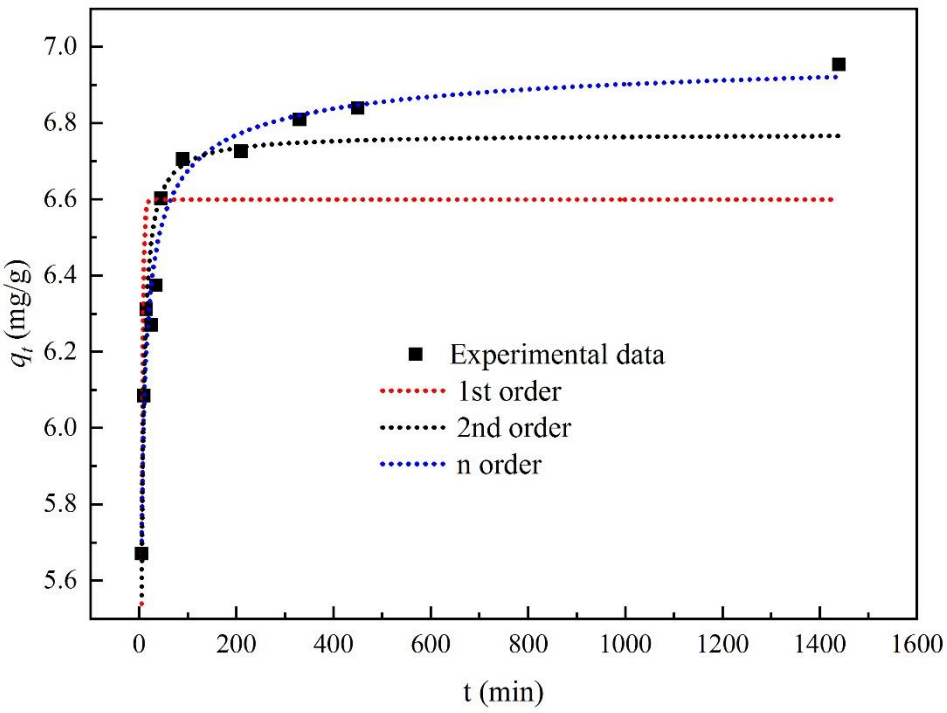

Figure 2-4. Adsorption kinetic curves (initial P concentration=50 mg/L, adsorbent dosage=5 g/L).

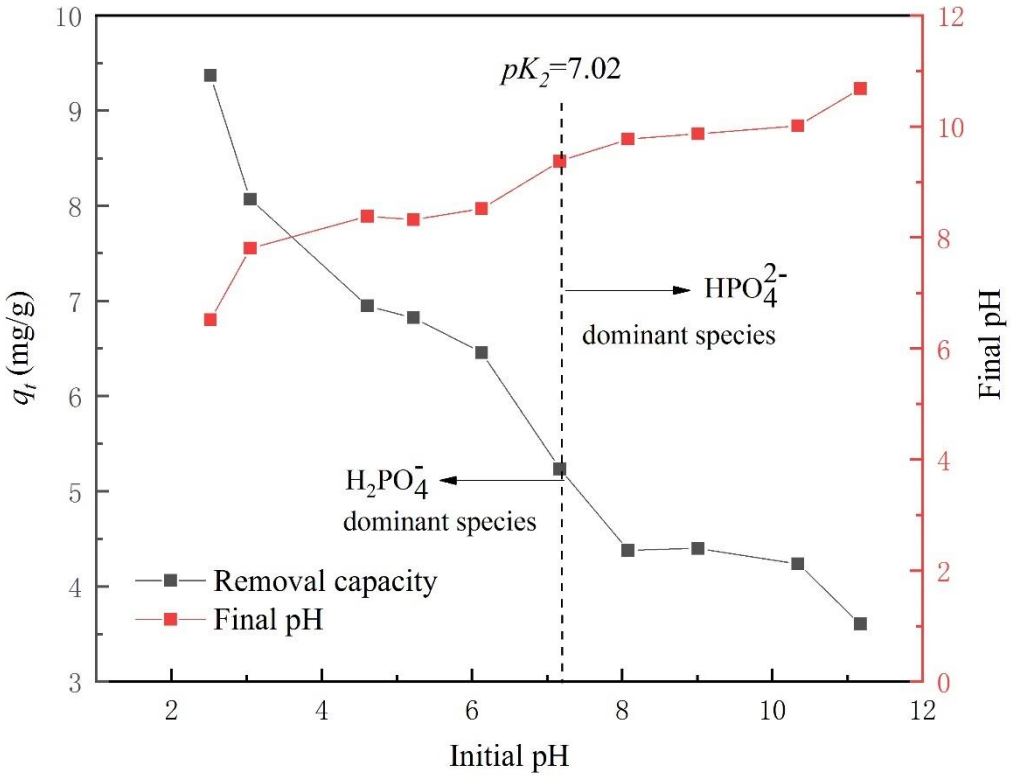

Figure 2-5. The effect of initial pH (initial P concentration=50 mg/L, adsorbent dosage=5 g/L).

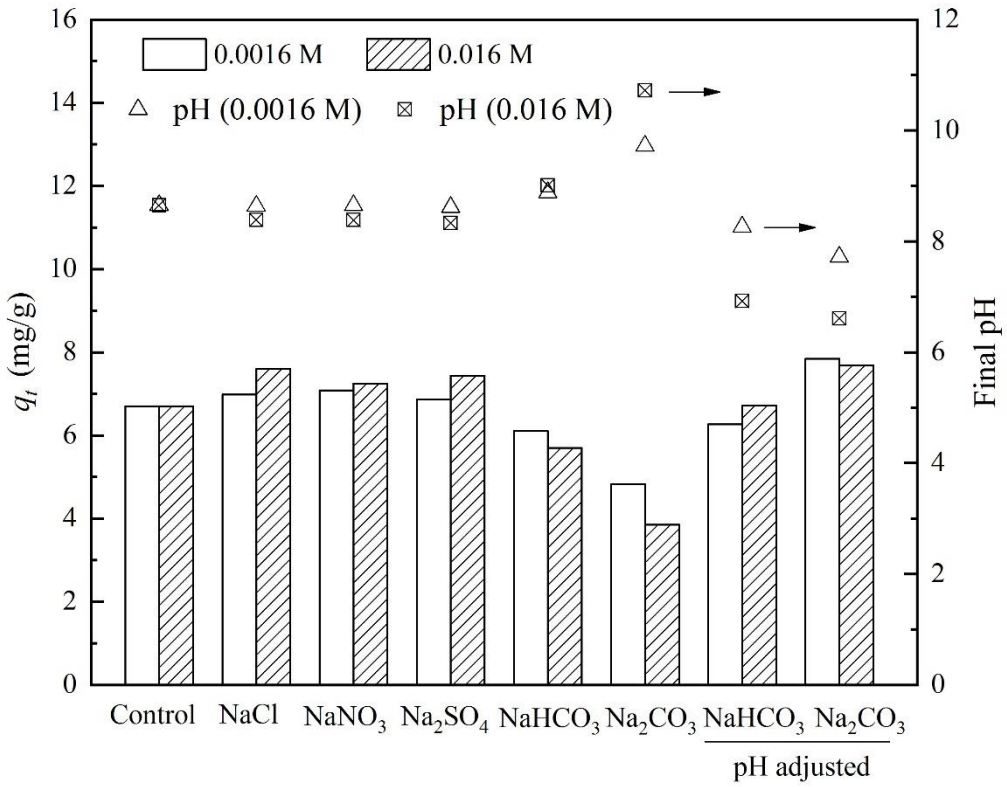

Figure 2-6. The effect of co-existing anions (initial P concentration=50 mg/L, adsorbent dosage=5 g/L).

Chapter 3 Efficient phosphate removal from wastewater by MgAl-LDHs modified hydrochar derived from tobacco stalk

3.1 Background

Phosphorous (P) is a basic nutrient for organisms and plays a critical role in agronomic production and industry development. The natural reserves for phosphate are limited and are estimated to be exhausted in 50–100 years (Zhang et al., 2016). On the other hand, excessive phosphorus discharge into aquatic environment from industrial, agricultural and domestic sources can cause eutrophication, which continues to be a seriously global issue (Pratt et al., 2012). Thus, phosphorus reclamation from phosphate-rich wastewater has been considered as a key strategy to prevent water quality from deterioration and simultaneously solve the phosphorus shortage issue (Desmidt et al., 2015).

Compared to various P control techniques such as ion exchange (Bui et al., 2018), chemical precipitation (Pratt et al., 2012), biological processes (Sun et al., 2015), crystallization (Shih et al., 2017), and electro-coagulation (Huang et al., 2016), adsorption has been recognized as one of the most attractive technologies owing to its simple operation, low cost, high removal efficiency, and potential for P reclamation from wastewater (Jiang et al., 2018; Zhang et al., 2019). Various types of adsorption materials, including natural minerals, metal-based materials, activated carbon, and engineering particles have been successfully developed to capture phosphate (Yang et al., 2014; Shi et al., 2019; Jiang et al., 2018). In fact, most of them are rather complicated in preparation, high cost or not so efficient (Jung et al., 2015b; Wan et al., 2017). Thus, renewable agricultural by-products are attracting increasing interest, which can be developed as low-cost and sustainable adsorbents with higher adsorption affinity for P removal/recovery. A number of methods have been reported on modification of agricultural by-products for better P decontamination, including quaternization, sulphate coating, metal loading, chemical and steam activation (Nguyen et al., 2014). However, these methods have some deficiencies like large consumption of chemicals, equipment erosion, specialized equipment, relatively complicated process and high cost (Nguyen et al., 2014). Hence, it is highly desirable to explore a facile and effective strategy for surface modification on agricultural waste.

With its high economic value, tobacco has been planted widely in many countries such as Brazil, China, USA, India, etc. (Ghosh and Reddy, 2013). As it is known, tobacco industry generates a huge amount of stalk biomass annually (about 1,000 kg ha^{-1}), the primary byproduct

waste after tobacco leaf being harvested. It is estimated that the annual generation of tobacco stalks is about 2.43 Mt in China (Ghosh and Reddy, 2013; Lin et al., 2016). Unfortunately, the great majority of tobacco stalks (TS) are burned off or discarded as solid waste after tobacco leaf being reaped (Li et al., 2008), causing considerable environmental contamination. Therefore, it is critical to explore the effective utilization potentials for TS wastes. As reported, TSs via carbonization can be converted to biochar or activated carbon, and used for pollutants adsorption including phosphine (Yi et al., 2013), heavy metals (Zhang et al., 2018) and organics (Mudyawabikwa et al., 2017). Most recently, hydrochar has been claimed to possess high potentials for pollutants adsorption (Fang et al., 2018). It's worth noting that the preparation condition for hydrochar (180°C−250°C) by hydrothermal carbonization (HTC) (Méndez et al., 2019) is milder than the preparation of biochar (300°C−700°C) through pyrolysis (Novak et al., 2013). In addition, the functionalization of hydrochar can be performed simultaneously during the HTC process, thus the one-step production/functionalization of hydrochar procedure can not only reduce the complexity of the production process, but also decrease the production costs compared to biochar or activated carbon-based adsorbents (Guo et al., 2017; Fang et al., 2018). Another attractive feature of hydrochar is that this kind of carbon-based adsorbents have been regarded as soil amendments (Fang et al., 2018). Restated, hydrochar adsorbents loaded with P nutrients can be utilized as slow-release fertilizers for agriculture, exhibiting positive effects on the restoration of soil ecosystem and carbon sequestration (Jung et al., 2015b). However, few attempts have been made to test the functionalized hydrochar materials for P removal/recovery.

Layered double hydroxides (LDHs) are a type of hydrotalcite-like materials or anionic clays (Goh et al., 2008; Li et al., 2016b). After partial substitution of divalent metal by trivalent metal and formation of positively charged layers of LDHs, the interlayer anions charged neutrality can be exchanged with various anionic species (Lǔ et al., 2013). With a high charge density of the sheets, large surface area and easily exchangeable interlayer ions, LDHs exhibit promising anionic pollutants capture affinity, such as anionic metal complexes, non-metal oxyanions, organic anions and anionic polymers (Goh et al., 2008). Many researches have examined the adsorption of phosphate onto LDHs. Das et al. (2006) investigated the phosphate adsorption capabilities of various calcined LDHs from aqueous system. Seida and Nakano (2002) demonstrated that above 80% of the phosphate in a drain effluent (0.2 mg P/L) could be removed by the synthesized Mg–Fe LDHs composite. Although LDHs can effectively capture phosphate from aqueous solution, they also have some drawbacks like weak hydraulic conductivity and tight layer stacking with generally slow and pH restriction (Barca et al., 2012;

Wan et al., 2017). Thus, the LDHs doped hydrochar composites could achieve enhanced activity in P adsorption compared to the pristine hydrochar, while during the HTC process, the surface and porous channels of hydrochar can supply a large reactive area for metal ions to nucleate metal oxides or hydroxides precipitation (Hug et al., 2001). Hence, the porous structure and abundant functional groups of hydrochar are also beneficial for the metal decoration and phosphate capture.

Up to the present, the preparation of functionalized hydrochar from TSs and its utilization on P removal have not been reported. In the present work, the TS-LDHs composite was prepared through carbonization of TS feedstock under hydrothermal conditions, serving as a sustainable supporting material that was modified simultaneously through a self-assembly synthesis of MgAl-LDHs to develop an effective and cost-efficient P removal adsorbent. Four main specific objectives were expected to realize in this work: (1) to compare the phosphate removal potentials of the resultant hydrochar composite modified by different ratio of MgAl-LDHs without and with CO_3^{2-} in the interlayer space; (2) to characterize the physicochemical properties of the resultant TS-LDHs composite that possessed the highest phosphate adsorption capability; (3) to evaluate the phosphate removal efficiency with varying parameters with respect to environmental conditions, including initial solution pH, adsorbent dosage, contact time, temperature and the initial phosphate concentration; and (4) to investigate the correlation coefficients regarding the kinetics, isotherms and adsorption mechanisms.

3.2 Materials and methods

3.2.1 Materials

Monopotassium phosphate (KH_2PO_4), sodium hydroxide (NaOH), magnesium chloride hexahydrate ($MgCl_2 \cdot 6H_2O$), aluminum chloride ($AlCl_3$) and other required chemicals were obtained from Wako Pure Chemical Industries Ltd., Japan, and all of them were in analytical grade. Deionized water (DW) was used to prepare all the experimental solutions and clean samples.

Tobacco stalk (TS) as the feedstock of hydrochar was collected from a local farm in Yunnan Province, China. The TS was washed, dried, then chopped and grinded, and finally sieved through 80 meshes before use.

3.2.2 Preparation and screening of TS-LDHs composite

The TS-LDHs composite was prepared through carbonization of TS feedstock under hydrothermal conditions, which combined the self-assembly synthesis of MgAl-LDHs according to a previous report (Yang et al., 2014). Varying amount of TS feedstock (0, 10 and 20 g) was added to a 100 mL DW solution containing 0.01 mol $AlCl_3$ and 0.03 mol $MgCl_2$, and then the pH of the mixture was adjusted to 10 by dropwise addition of different alkaline solution containing 1 M NaOH or 1M NaOH and 0.5 M Na_2CO_3, respectively. The mixture was then transferred to a stainless steel autoclave (200 mL) and heated at 180 °C for 12 h. The resultant slurry in the autoclave was filtered using a Whatman Filter Paper Grade 42, then rinsed with DW. After the filtrate being dried over night at 80°C, the TS-LDHs samples were obtained. The concentrations of Al and Mg in the filtrate were quantified using ICPS (Shimadzu ICPS-8100, Japan), and the mass of loaded Al/Mg was calculated according to the amount reduction after HTC process. Raw hydrochar and MgAl-LDHs samples were prepared through the same procedure but without the addition of metal solution or TS feedstock, respectively.

Experiments on phosphate removal potentials of different TS-LDHs were carried out in 50 mL centrifuge tubes containing 20 mL solution of 50 mg P/L and 0.1 g of each adsorbent. After 24 h adsorption, phosphate concentrations were detected using the same method as in section 2.4. The MgAl-LDHs modified hydrochar with the highest phosphate removal amount in these experiments was selected for further study.

3.2.3 Characterizations

The morphological appearance and structure features of the TS-LDHs samples were characterized by scanning electron microscopy (FEG-SEM, Nova NanoSEM 450) and transmission electron micrograph (JEM-2011, Japan). Fourier transform infrared (FTIR) spectra were recorded using a Thermo Fisher model Nicolet iS5 in ATR mode. Surface areas of the original hydrochar and TS-LDHs samples were analyzed with a Quantachrome Uadrasorb-evo surface area analyzer using the N_2 (BET) adsorption method. Bruker AXS Inc D8 ADVANCE was used for taking the powder XRD patterns to determine the crystallographic structure of the samples. The EDS was performed to characterize the composition and element contents of the TS-LDHs composites before and after P adsorption by an Electron-probe microanalyzer (JXA-8230, Japan).

3.2.4 Effects of environmental conditions on P adsorption

Batch adsorption experiments were conducted using 50 mL centrifuge tubes to assess the influences of various environmental factors on P adsorption. For the effect of initial pH, the pH value of the mixture (0.1 g composite in 20 mL of 50 mg P/L solution) was adjusted to 2, 4, 6, 7, 8, 10, and 12 with different amounts of 0.1M NaOH or HCl solution. The final pH values of the suspensions were also detected. For the effect of adsorbent dosage, 0.02, 0.06, 0.10, 0.14, 0.18, 0.22, 0.26 or 0.30 g composite was mixed with 20 mL of 50 mg P /L phosphate solution. For the effects of co-existing anions, 20 mL of 0.0016 M or 0.016 M NaCl, $NaNO_3$, $NaHCO_3$, Na_2SO_4, or Na_2CO_3 with an initial P concentration of 50 mg P/L solution was mixed with 0.1 g composite. Thus, the concentrations of competitive anions (chloride, nitrate, bicarbonate, carbonate and sulfate) were about equal or 10 times greater than that of phosphate on a molar basis.

After above steps, the mixtures were shaken at 120 rpm and room temperature (25±2 °C). After 24 h, all the mixtures were filtered and phosphate concentrations in the filtrates were detected with the ascorbic acid method (4500-P E) (APHA, 2012). All the measurements were conducted in duplicate, with average values being presented. Additional trials were carried out, until a difference between two test values were less than 5%. Phosphate removal capacity was calculated as follows:

$$q_e = (C_i - C_e) \times V/m \quad (3\text{-}1)$$

where q_e is the amount of phosphate adsorbed onto per unit weight of adsorbent (mg/g), V is the solution volume (L), C_i and C_e are the initial and equilibrium phosphate concentrations (mg/L), respectively, and m is the mass of the adsorbent (g).

3.2.5 Adsorption kinetics and isotherms

The adsorption isotherms and the effect of temperature on phosphate adsorption were studied. Series of 0.1 g TS-LDHs composite were mixed with 20 mL solutions with different initial phosphate concentrations ranging from 5 to 800 mg P/L. A temperature thermostat was used to ensure different reaction temperatures (25, 35 and 45 °C). After 24 h, phosphate concentrations were detected with the same method in section 3.2.4.

Phosphate adsorption kinetics on the TS-LDHs composite were determined by adding 1 g TS-LDHs composite to 200 mL of different initial phosphate concentration (10 or 50 mg /L) solution in 500 mL Erlenmeyer flasks. The mixture was then shaken at 120 rpm and room temperature (25±2 °C) in a mechanical shaker. The suspensions (0.5 mL) were collected at 5,

10, 20, 30, 50, 60, 120, 180, 240 and 300 min, respectively and their P concentrations were measured using the method mentioned in section 3.2.4.

3.3 Results and discussion

3.3.1 Phosphate removal potentials of different TS-LDHs composites

Four composites were obtained by co-precipitation of MgAl-LDHs with or without CO_3^{2-} in the interlayer space on varying amounts of TS feedstock. Phosphate adsorption ability of the different TS-LDHs composites and the pristine hydrochar were compared and the results are shown in Fig. 3-1. The hydrochar derived from TS without any modification exhibited very limited phosphate removal capability (0.02 mg/g), while the adsorption capability of TS-LDHs composite increased obviously to 1.78 - 5.07 mg P/g, confirming the functional enhancement on phosphate affinity of the hydrochar by MgAl-LDHs. The improvement of the MgAl-LDHs on phosphate adsorption was evidently revealed by the apparent increasing trend in the adsorbed phosphate amount with the increase of MgAl-LDHs content (reducing TS feedstock amount). As the hydrochar derived from 10 g TS feedstock modified by MgAl-LDHs without CO_3^{2-} in the interlayer space exhibited the best phosphate adsorption capability, it was selected for the followed-up phosphate removal study. In order to further elucidate the effect of MgAl-LDHs on phosphate adsorption by hydrochar, pure MgAl-LDHs composite was also synthesized. The phosphate adsorption amount on the pure MgAl-LDHs was visibly higher than other composites; however, if normalized on the weight basis of Mg/Al loaded, the adsorption capacity per unit weight of MgAl-LDHs in hydrochar was higher than that of pure MgAl-LDHs, indicating a synergetic effect between hydrochar and MgAl-LDHs.

3.3.2 Characterization

The XRD patterns of raw hydrochar, TS-LDHs and Mg/Al-LDHs are illustrated in the Supplementary Materials (Fig. 3-2). A series of peaks as sharp and intense symmetric lines at low 2θ values and clear reflections at high 2θ values were observed from the XRD patterns of Mg/Al-LDHs, which resembles the typical XRD pattern of a pure hydrotalcite (Halajnia et al., 2013). When the patterns of the TS-LDHs and raw hydrochar being compared, the appearance of diffraction angles at 2θ=10.7° and 34.6 ° corresponding to the crystal surface of MgAl-LDHs (Wang et al., 2008) suggested the adhesion of Mg/Al-LDHs to the surface of hydrochar.

SEM was performed to study the surface morphology of the pristine tobacco stalk and TS-LDHs composite. In the Supplementary Materials (Fig. 3-3a), the raw TS exhibited a uniformly

ordered smooth structure with many irregular small fragments on the surface. However, TS-LDHs composite (Fig. 3-3b) reflected a large amount of cracks and gullies on the surface, which were coated with numerous coarse lamellar particles. Furthermore, the microstructures of raw hydrochar, MgAl-LDHs and TS-LDHs composite were also characterized by TEM. As illustrated in the Supplementary Materials (Fig. 3-4), TS-LDHs composite is formed by regular agglomerates of tiny disk-like particles, ranging in several tens to hundreds of nanometers. In contrast, MgAl-LDHs exhibitates unique clusters of polygon layer structure at a smaller size. Compared to the raw hydrochar, TS-LDHs composite exhibited obvious increase in fragmentation and porosity, indicating the formation of LDHs sheets on the hydrochar matrix. Hydrochar can serve as a supporting material for LDHs dispersion during the synthesis, resulting to the functional improvement on active sorption sites (Wan et al., 2017). The results were consistent with the results from BET surface area analysis (Table 3-1). The surface area, pore volume and diameter of TS-LDHs composite were about 13, 17 and 3 times that the raw TS, respectively. After phosphate adsorption, the pore volume, surface area and diameter of TS-LDHs composite were slightly decreased. In addition, the pore volume and surface area of MgAl-LDHs were much higher than the raw TS, contributing to the rough and porous surface of TS-LDHs composite.

The FTIR spectra of raw TS, hydrochar, MgAl-LDHs, and TS-LDHs composite before and after phosphate adsorption (in the kinetics study experiments) are shown in Fig. 3-5. TS-LDHs composite produced in this study was abundant in oxygen containing functional groups which could support chemical or physicochemical adsorption (Li et al., 2018b). Sharp decrease was observed at the bands around 3360 cm^{-1} and 1616 cm^{-1} (associated with the stretching vibrations O–H in carboxyl or hydroxyl groups) , 2920 cm^{-1} (contributed to the C-H stretching vibration of cellulose), and the broad band between 1160–896 cm^{-1} (associated with C–O stretching vibration of glycosidic linkages). The absorbance bands around 1745 and 1250 cm^{-1} (ascribed to the C=O stretching vibration) disappeared after hydrothermal carbonization. The decline of these corresponding bands suggests that dehydration and hydrolysis reaction occurred during the HTC process. Benzene peaks around 1610 and 1520 cm^{-1} were found in the raw TS and TS-LDHs composite, implying that the aromatic structure relating to lignin is stable at < 200℃. Compared to the functional groups of MgAl-LDHs, the bands at 1352 cm^{-1} and in the 400–500 cm^{-1} region of TS-LDHs composite might be contributed by the O–H vibrations of metal oxides (M–OH) and metal–oxygen bonds M–O (M=Mg, Al) vibration

(Biswas et al., 2008), respectively. The results from the FTIR spectra of TS-LDHs composite verified the presence of the LDHs in the hydrochar composites.

3.3.3 Effect of environmental conditions on phosphate adsorption

Batch adsorption experiments were carried out to evaluate the influences of various environmental conditions on phosphate removal. The phosphate removal efficiency by the TS-LDHs composite at varying adsorbent dosages (1–15 g/L) is shown in Fig. 3-6. The phosphate uptake amount decreased from 12.5 mg P/g (at the dosage of 1 g/L) to 3.14 mg P/g (at the dosage of 15 g/L), while the phosphate adsorption efficiency significantly increased from 24.7% to 93.03%. As seen, the phosphate removal efficiency increased obviously with the increase of TS-LDHs composite dose from 1 to 7 g/L, thereafter increased slightly and tended to remain stagnant at the TS-LDHs composite dosage of 15 g/L. This observation is attributable to the greater amount of approachable active adsorption sites and surface area provided by the TS-LDHs composite (Zhang et al., 2019). When less TS-LDHs composite was dosed, limited active sites were available leading to the lower phosphate uptake capacity.

As shown in Fig. 3-7, phosphate adsorption onto the TS-LDHs composite exhibited the largest capacity (8.75 mg P/g) at an initial pH 2, and then a downward trend was observed with the increase of initial pH. The phosphate removal capacity was decreased by only 2.08%-17.5% with the increase of initial solution pH from 4 to 8, which was decreased rapidly when the initial pH value was further raised to 12. Results from Fig. 3-7 show that although a lower solution pH is more favorable for phosphate removal, TS-LDHs composite is also efficient in phosphate adsorption under both neutral and slightly alkaline conditions. The observation can be explained by the acidic-basic surface properties of adsorbent and the pH-dependent phosphate dissociation equilibrium as follows (Das et al., 2006):

$$H_3PO_4 \overset{pK_1=2.15}{\longleftrightarrow} H_2PO_4^- + H^+ \overset{pK_2=7.20}{\longleftrightarrow} HPO_4^{2-} + 2H^+ \overset{pK_3=12.33}{\longleftrightarrow} PO_4^{3-} + 3H^+ \qquad (3\text{-}2)$$

For a detailed description, when the solution pH ranges from 2.15 to 7.20, the predominant species is $H_2PO_4^-$; while in the pH ranging from 7.20 to 10.0, the main species is HPO_4^{2-} (Zhang et al., 2019). $H_2PO_4^-$ possesses a lower adsorption free energy compared to HPO_4^{2-}, resulting in more easily capture of $H_2PO_4^-$ onto the surface of adsorbent (Jiang et al., 2018). Besides, the surface of TS-LDHs composite is protonated and becomes positively charged at lower pH favoring electrostatic attraction. Meanwhile, hydroxyl ions could compete with phosphate species and occupy the available active adsorption sites, therefore reducing the phosphate removal capability at higher pHs (Lǔ et al., 2013; Yan et al., 2015; Jiang et al., 2018).

Noticeably, as illustrated in Fig. 3-7, the final pH value of mixture (6.75-8.26) was higher than the initial pH ranging from 2 to 8, indicating hydroxyl ions were released into the solution after the interaction between adsorbent and adsorbate. While when the initial pH value was 10 or 12, the final solution pH was 8.36 or 11.17, indicating the buffering capability of TS-LDHs composite during phosphate adsorption.

The coexistence of oxyanions may typically compete with phosphate in wastewater (Li et al., 2016c). Therefore, the influence of the commonly coexisting anions (including Cl^-, NO_3^-, SO_4^{2-}, CO_3^{2-}, and HCO_3^-) on phosphate removal was investigated as shown in Fig. 3-8. Results indicate that Cl^- and NO_3^- had very limited competitive effect. The coexistence of HCO_3^- or SO_4^{2-} showed negative effect on phosphate removal. When the concentrations of the competing anions were raised from 0 to 0.0016 M and further to 0.016 M, the reductions in phosphate adsorption amount were 6.74% and 20.9% in the coexistence of SO_4^{2-}, and 8.51% and 31.2% in the presence of HCO_3^-, respectively. CO_3^{2-} exhibited a relatively strong competition effect on phosphate removal, which reduced the phosphate adsorption amount by 25.5% and 78.4% when its concentration was increased from 0 to 0.0016 M and to 0.016 M, respectively. Overall, the impact of the tested anions on phosphate adsorption followed a descending order as carbonate > bicarbonate > sulfate > nitrate ≥ chloride.

Since the addition of oxyanions may change pH which plays a critical role on phosphate adsorption, the final solution pH was also determined. Results show that addition of SO_4^{2-}, Cl^- or NO_3^- did not change pH substantially while addition of CO_3^{2-} and HCO_3^- induced a significant increase in pH, which should be taken into account when analyzing their strongly negative effects on phosphate adsorption on the prepared composite.

3.3.4 Adsorption kinetics

The adsorption experiments of phosphate onto the TS-LDHs composite were conducted as a function of contact time at different initial phosphate concentrations (10 mg/L or 50 mg/L). As clearly seen in Fig. 3-9, the two curves exhibited a similar trend and progressed rapidly, reaching its equilibrium within 1 h, which was faster than other carbon-based phosphate adsorbents (Yao et al., 2011). In order to interpret the mechanisms involved, two different kinetic models were used and their corresponding equations are as follows (Yao et al., 2011):

Pseudo-first-order model: $q_t = q_e(1 - e^{-K_{P1}t})$ (3-3)

Pseudo-second-order model: $q_t = \frac{K_{P2}q_e^2 t}{1+K_{P2}q_e t}$ (3-4)

where K_{P1} and K_{P2} represent the rate constants for the pseudo-first-order model (min^{-1}) and pseudo-second-order model (g/(mg min)), respectively. q_t and q_e are the uptake amount of P for per unit adsorbent weight at a certain time *t* and at equilibrium (mg/g), respectively.

The corresponding kinetic parameters are summarized in Table 3-2. The obtained correlation coefficients (R^2) of the pseudo-second-order model (0.9997 and 0.9994) are greater than those of the pseudo-first-order model (0.9927 and 0.9788). Thus, the adsorption of phosphate onto TS-LDHs composite might be dominated by chemisorption processes involving chemical bonding between the adsorbent active sites and phosphate (Yang et al., 2014). Moreover, the rate constants of the pseudo-second-order model (K_{P2}) were 0.0258 and 0.332 g/(mg min) at the initial phosphate concentrations of 10 and 50 mg/L, respectively, indicating the TS-LDHs composite possesses a faster removal rate at a lower initial phosphate concentration and could achieve equilibrium in a shorter time. Besides, the calculated rate constants (K_{P2}) were larger than other reported metal (hydr)oxides incorporated biomass derived adsorbents, such as 0.112 g/(mg min) for Mg–Al LDHs modified biochar (Wan et al., 2017) and 0.013 g/(mg min) for Mg–Al–La (hydr)oxides functionalized zeolite (Shi et al., 2019) at an initial phosphate concentration of 10 mg/L. The results revealed that a shorter time is required for TS-LDHs composite to remove phosphate effectively from wastewater containing a certain concentration of phosphate.

3.3.5 Adsorption isotherms: effect of reaction temperature

The phosphate adsorption equilibrium isotherms of the prepared TS-LDHs composite was studied at 25, 35 and 45°C, respectively. The data obtained from the experiments were evaluated using the Langmuir and Freundlich isotherm models (Jung et al., 2016) as follows:

Langmuir isotherm model: $q_e = \frac{q_m K_L C_e}{1 + K_L C_e}$ (3-5)

Freundlich isotherm model: $q_e = K_F C_e^{1/n}$ (3-6)

where K_L and K_F denote the constants of Langmuir and Freundlich models, respectively. q_m is the maximum phosphate uptake capacity and n represents the heterogeneity factor.

The fitted isotherm curves and the corresponding parameters are summarized in Fig. 3-10 and Table 3-3, respectively. Taking the correlation coefficient values into consideration, the Freundlich equation (R^2 = 0.994, 0.995 and 0.994) exhibited a better fitting than the Langmuir equation (R^2 = 0.961, 0.962 and 0.970). The calculated maximum adsorption capacities by the Langmuir model were 30.7, 31.4 and 41.2mg P/g at 25, 35 and 45 °C, respectively, which were

much higher than the previously reported adsorbents (Table 3-3). In addition, the increase in adsorption ability with the increase of reaction temperature suggests that a higher temperature is beneficial for phosphate adsorption onto TS-LDHs, resulting in stronger interaction forces between phosphate species and the adsorbent (Jung et al., 2015a). The above result reveals that phosphate adsorption onto TS-LDHs composite is an endothermic process, which could be chemical interactions rather than physical ones.

3.3.6 Mechanisms analysis

(1) Electrostatic attraction

FTIR spectra confirmed the existence of metal oxides (M–OH) and some metal–oxygen bonds M–O (M=Mg, Al) vibration on the TS-LDHs composite. At low pH conditions, the existence of numerous H^+ ions can induce the protonation of adsorbent surfaces containing metal hydroxide, and the adsorbents are positively charged. At a high pH value, metal hydroxides are deprotonated with resultant in negatively charged adsorbent surfaces. The process can be illustrated as follows:

$$M - OH + H^+ \leftrightarrow M - OH_2^+ \quad (3\text{-}7)$$

The positively charged groups on the surface of TS-LDHs composite contribute to the electrostatic attraction as an important mechanism for capture of the negatively charged phosphate species.

(2) Ligand exchange

When phosphate adsorption was performed at increasing initial solution pH from 2.0 to 10.0, the final solution pH after phosphate uptake fluctuated between 6.75 - 8.36. This could be explained by the ligand exchange between hydroxyl groups and phosphate species according to the following reactions (Yang et al., 2014; Shi et al., 2019):

$$M - OH + H_2PO_4^- \leftrightarrow M - H_2PO_4^- + OH^- \quad (3\text{-}8)$$

$$M = OH + HPO_4^{2-} \leftrightarrow M = PO_4^{2-} + OH^- \quad (3\text{-}9)$$

$$M \equiv OH + PO_4^{3-} \leftrightarrow M \equiv PO_4^{3-} + OH^- \quad (3\text{-}10)$$

Under low pH conditions, the negatively charged phosphate species can be easily attracted by the protonated adsorbent surfaces ($–MOH_2^+$), then exchange with hydroxyl groups and release OH^- through ligand exchange, which would cause the increase in solution pH. In addition, $-OH_2^+$ is easier to be replaced from the active sites than hydroxyl groups, leading to the acceleration of the ligand exchange process (Zhang et al., 2019). This phenomenon is consistent with the remarkable decrease of the FTIR spectra intensity associated with O–H

stretching vibrations of TS-LDHs composite after phosphate adsorption. With the increase in solution pH, the adsorbent surface can be deprotonated (-MO^-), which can adsorb the positively charged cations easily and release H^+. However, the existing high amount of OH^- may inhibit the ligand exchange with phosphate species. Thus, the released amount of H^+ is higher than that of OH^-, accounting for the decrease in final pH when adsorption equilibrium is reached.

(3) Ion exchange

In order to further reveal the mechanisms involved, electron-probe microanalysis was performed to analyze element contents of the TS-LDHs composite as shown in Fig. 3-11. It was observed that the percentages of Mg and Al atoms were respectively 2.25% and 0.9% at the near surface of pre-adsorption TS-LDHs composite. This means that Mg/Al molar ratio was about 2.5. The percentage of O was reduced by 2.25% after phosphate adsorption, which could be explained by the release of hydroxyl group during ligand exchange process. The percentage of P atoms in the pre-adsorption sample was 0.22%, since P is a basic nutrient for plant and generally exists in the raw biomass, raw tobacco stalk in this study. The result also shows that the percentage of P atoms increased in the post-adsorption sample. In addition, Cl atoms in the pre-adsorption sample decreased by 0.16% after desorption of phosphate. The replacement of Cl by P was in agreement with the characteristics of LDHs which have some easily exchangeable intercalation anions (Das et al., 2006), indicating that interlayer ion exchange is an important adsorption mechanism.

3.4 Summary

In this study, the TS-LDHs composites were prepared through a one-step HTC method with enhanced phosphate adsorption from aqueous solution in a wide pH range. The maximum adsorption capacity acquired by the Langmuir model was up to 41.16 mg P/g at 45 °C, much higher than many other adsorbents. The adsorption mechanisms involved are ion exchange, ligand exchange and electrostatic attraction. This study proposed an efficient alternative to utilize abundant agricultural organic solid wastes to produce promising adsorbents (like TS-LDHs composite in this study) for phosphate removal/recovery from wastewater.

Table 3-1. Summary of BET analysis results of raw tobacco stalk, TS-LDHs before and after phosphate adsorption.

	BET surface area (m^2/g)	Pore volume (cm^3/g)	Average pore diameter (nm)
Raw tobacco stalk	2.57	0.006	3.21
MgAl-LDHs	33.9	2.173	2.56
TS-LDHs	32.3	0.103	9.62
P-laden-TS-LDHs	29.1	0.093	9.60

Table 3-2. Kinetic parameters of phosphate adsorption onto TS-LDHs.

C_i (mg/L)	Pseudo-first-order			Pseudo-second-order		
	Kp_1 (min^{-1})	q_e (mg/g)	R^2	Kp_2 [g/(mg min)]	q_e (mg/g)	R^2
10	0.277	1.77	0.993	0.332	1.84	0.9997
50	0.0962	5.15	0.979	0.0258	5.57	0.9994

(Note: Other experimental conditions included initial P concentration=50 mg P/L, and adsorbent dosage=5 g/L)

Table 3-3. Freundlich and Langmuir constants and correlation coefficients for phosphate adsorption onto TS-LDHs.

Temperature (°C)	Langmuir			Freundlich		
	K_L (L/mg)	q_m (mg/g)	R^2	K_F [(mg/g)(L/mg)$^{1/n}$]	n	R^2
25	0.005	30.7	0.961	1.66	2.37	0.994
35	0.007	31.4	0.962	2.06	2.50	0.995
45	0.005	41.2	0.970	1.81	2.22	0.994

Table 3-4. Performance of other adsorbents for phosphate removal.

Adsorbent	Adsorption condition (°C; pH)	Dosage (g/L)	C_i (mg/L)	q_m (mg/g)	Ref.
Fe–Zr binary oxide	25; 4	1	0 - 100	13.7	Long et al. (2011)
Fe-Al binary oxide	–	–	10 - 200	16.4	Tofik et al. (2016)
Iron-doped activated carbon	15, 25, 35; –	2	11.82-42.96	7.31-15.3	Wang et al. (2012)
Peanut shell biochar	30; –	–	–	6.79	Jung et al. (2015a)
Sugar cane bagasse biochar	25; 7	2	25-400	2.95 -13.2	Trazzi et al. (2016)
Waste-marine macroalgae biochar	10-30; 7	1	1-200	20.9-32.6	Jung et al. (2016)

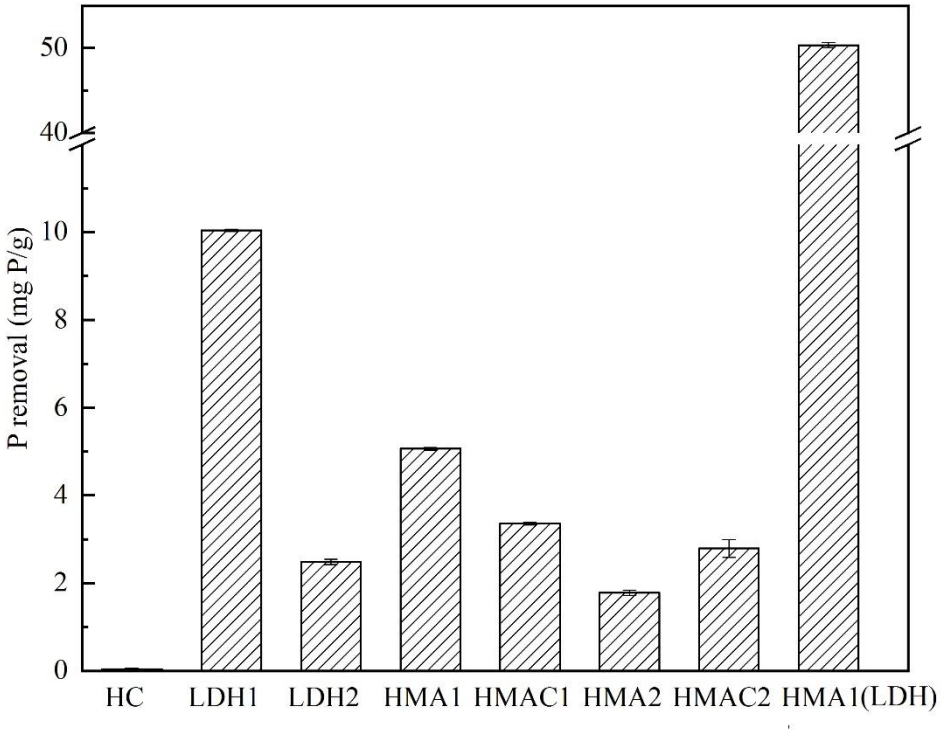

Figure 3-1. Phosphate removal potentials of different hydrochar/MgAl-LDHs composites (HC: pristine hydrochar; LDH1: pure MgAl-LDHs; LDH2: pure MgAl-LDHs with CO_3^{2-} in the interlayer space; HMA1 and HMAC1: hydrochar derived from 10 g TS feedstock modified by MgAl-LDHs without and with CO_3^{2-} in the interlayer space, respectively; HMA2 and HMAC2: homologous composites derived from 20 g TS feedstock modified by MgAl-LDHs without and with CO_3^{2-} in the interlayer space; HMA1(LDH): normalized on the weight basis of Mg/Al loaded.)

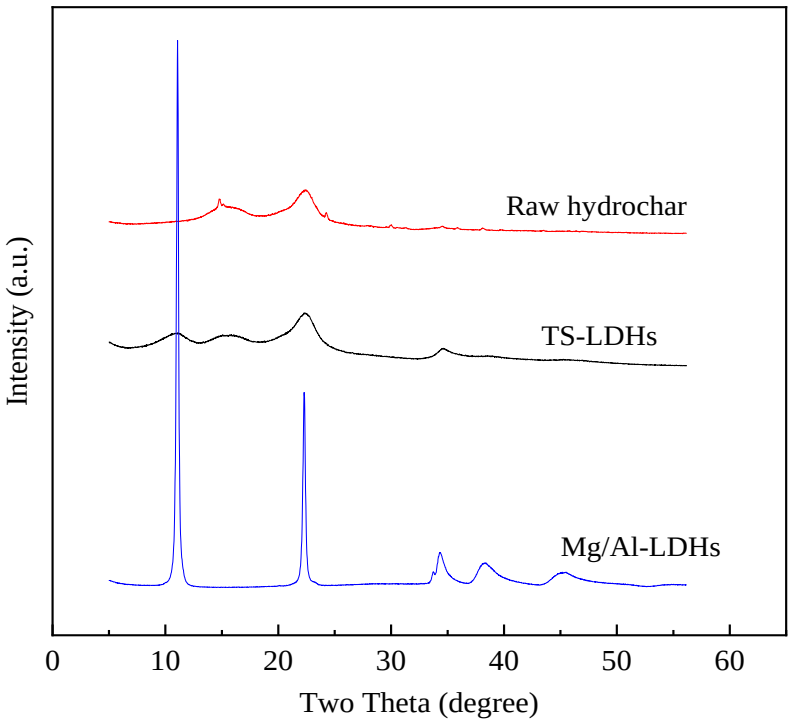

Figure 3-2. XRD patterns of raw hydrochar, TS-LDHs and MgAl-LDHs composite.

(a)

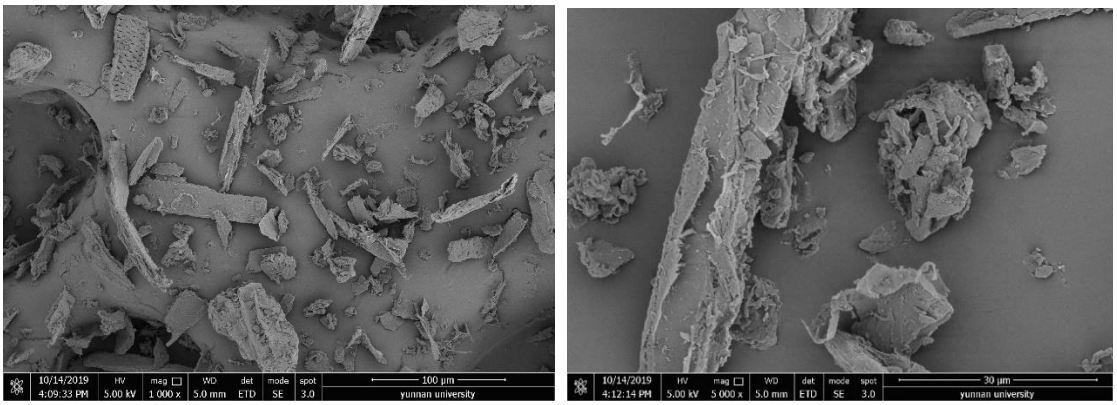

(b)

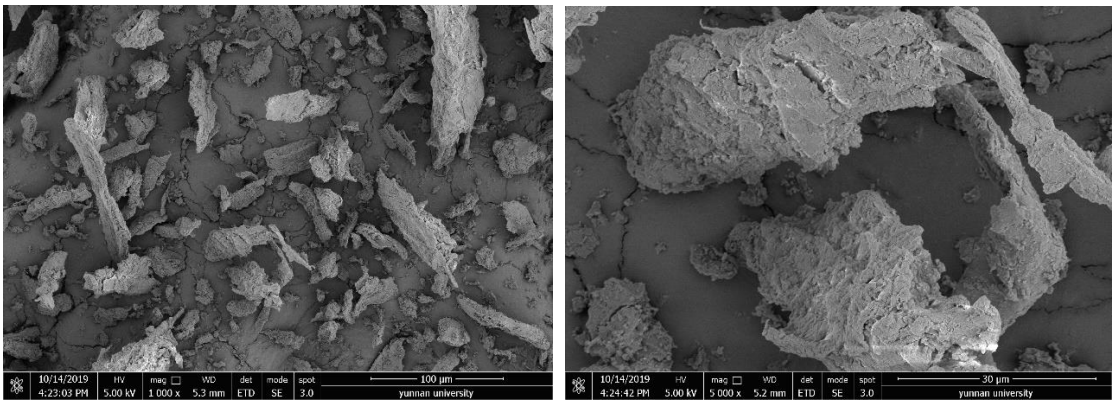

Figure 3-3. SEM images of raw tobacco stalk (a) and TS-LDHs composite (b).

(a)

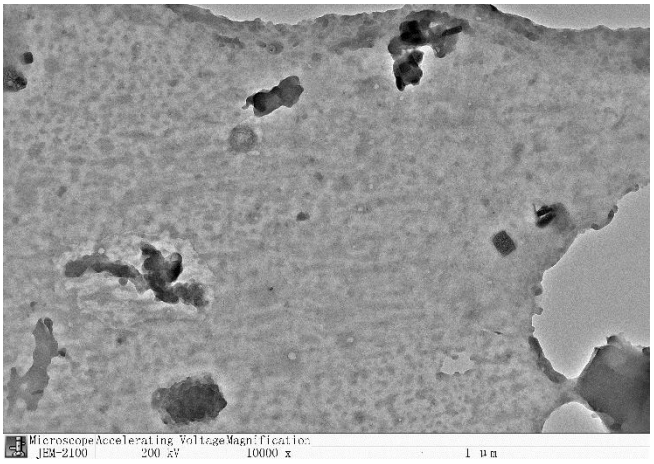

(b)

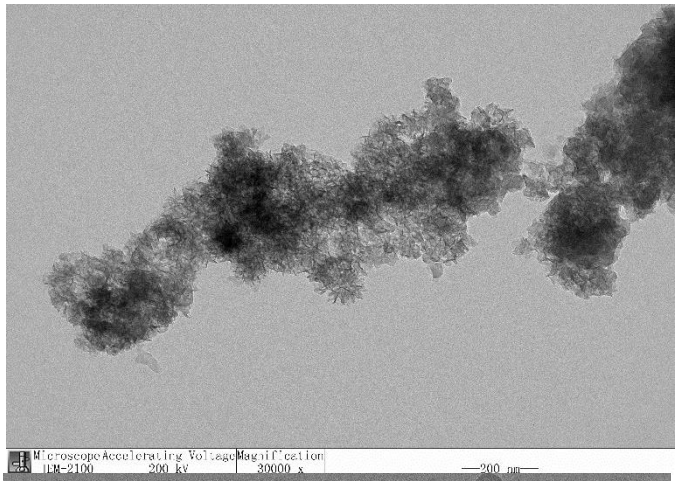

(c)

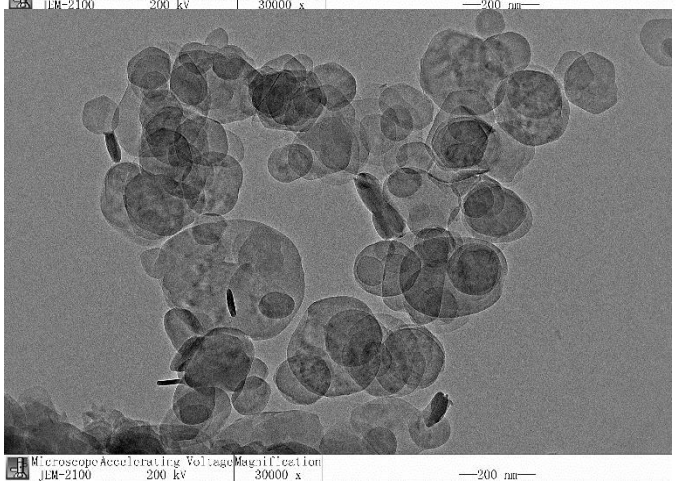

Figure 3-4. TEM images of raw hydrochar (a) MgAl-LDHs (b) and TS-LDHs composite (c).

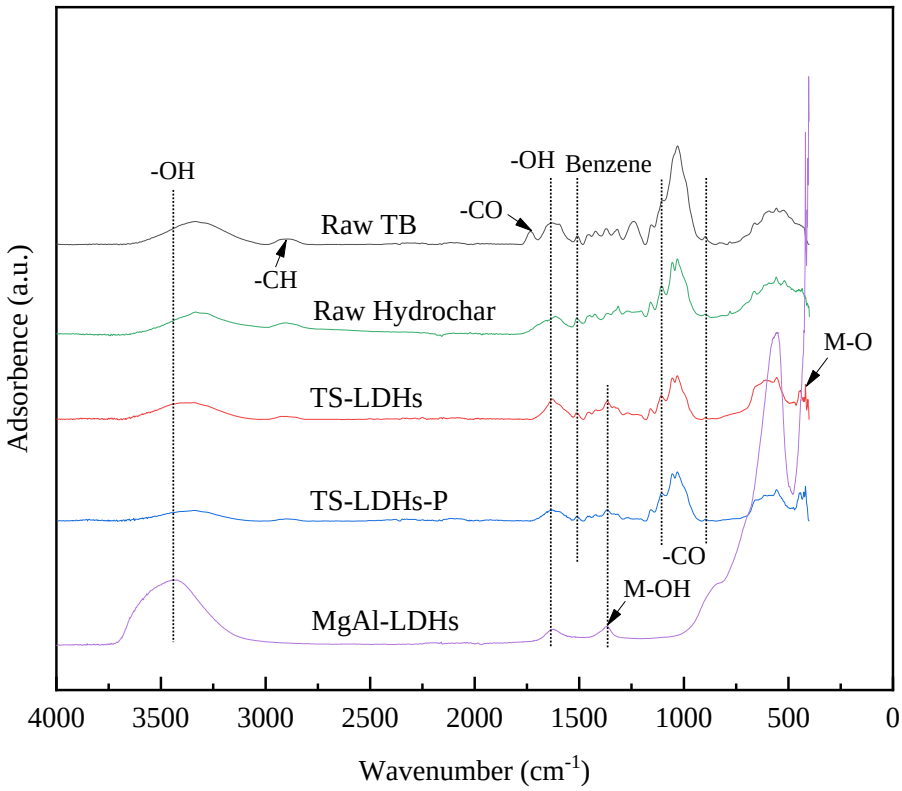

Figure 3-5. FTIR spectra of raw tobacco stalk, hydrochar, MgAl-LDHs, TS-LDHs before and after phosphate adsorption.

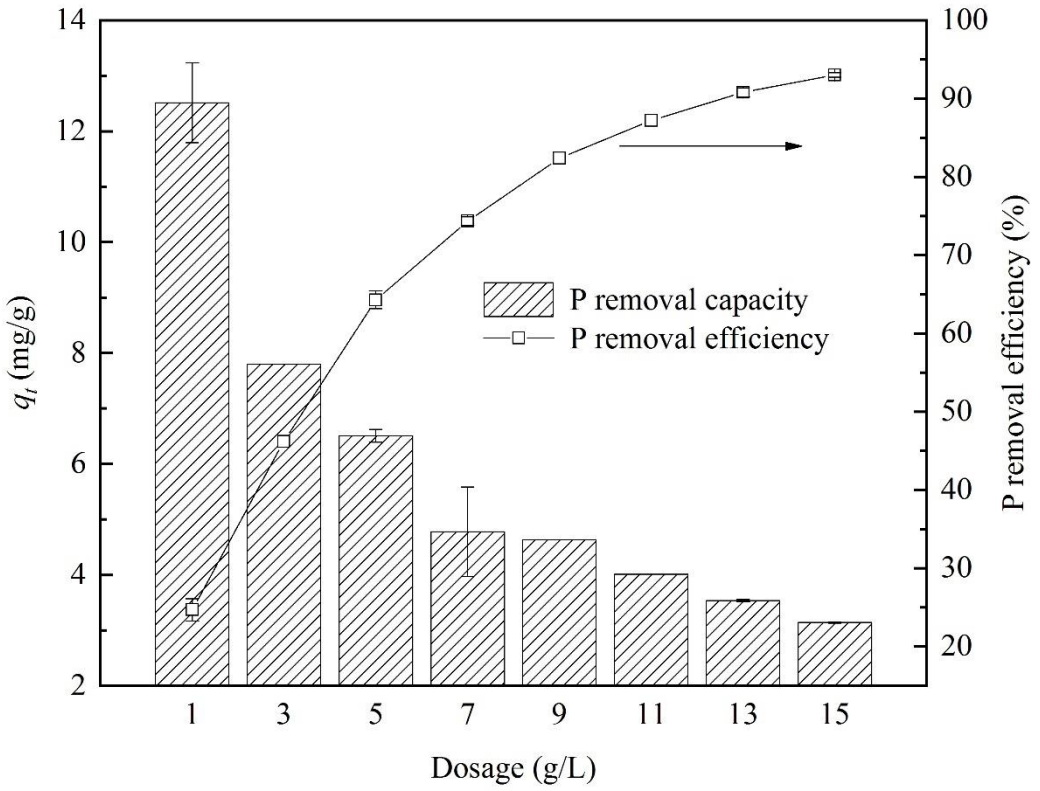

Figure 3-6. The effect of adsorbent dosage on the prepared composite. (Initial P concentration=50 mg/L)

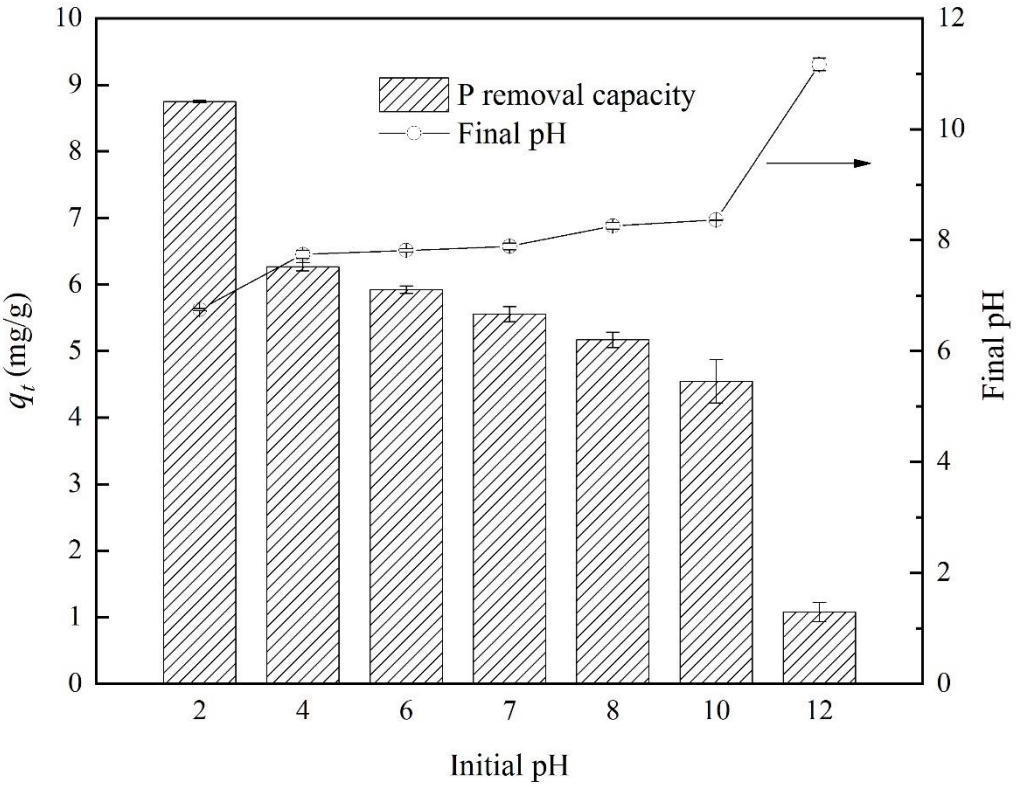

Figure 3-7. The effect of initial solution pH on the prepared composite. (Initial P concentration=50 mg/L, adsorbent dosage=5 g/L)

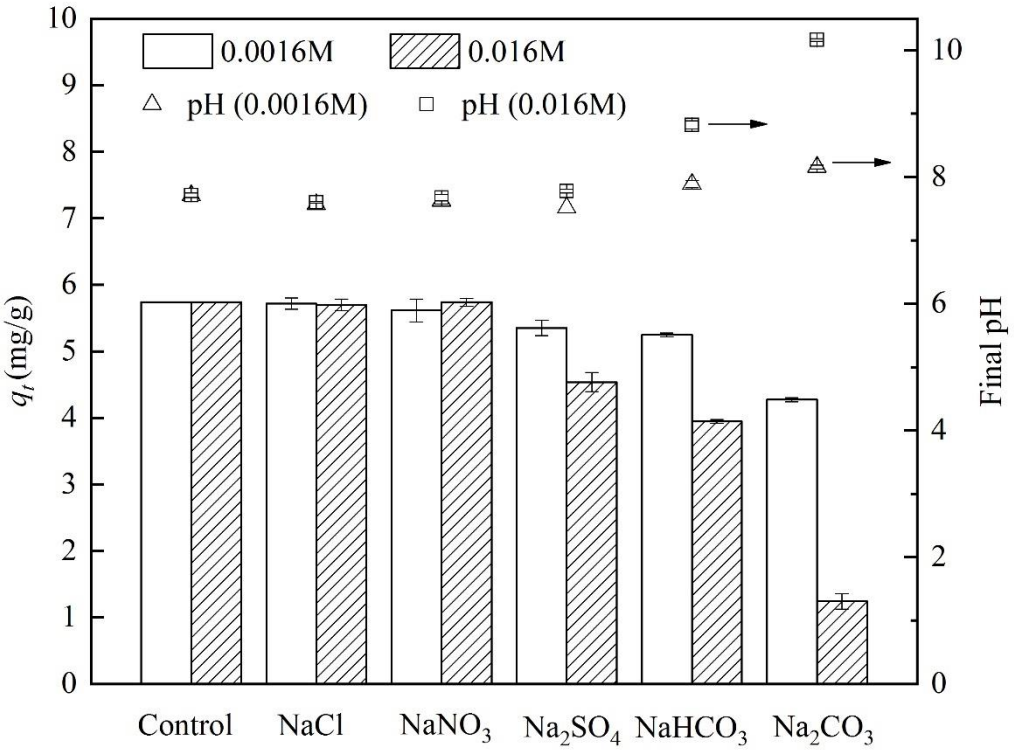

Figure 3-8. The effect of co-existing anions on P adsorption onto the prepared composite. (Initial P concentration=50 mg/L, adsorbent dosage=5 g/L)

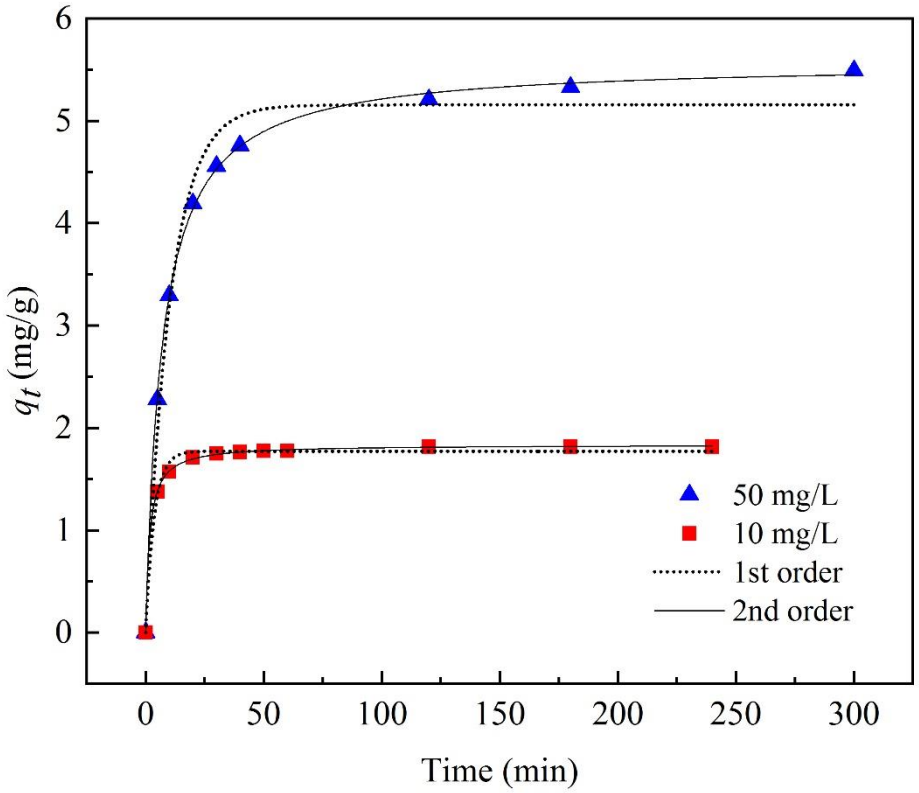

Figure 3-9. Adsorption kinetics of phosphate adsorption onto TS-LDHs. (initial P concentration = 10/50 mg/L,adsorbent dosage=5 g/L)

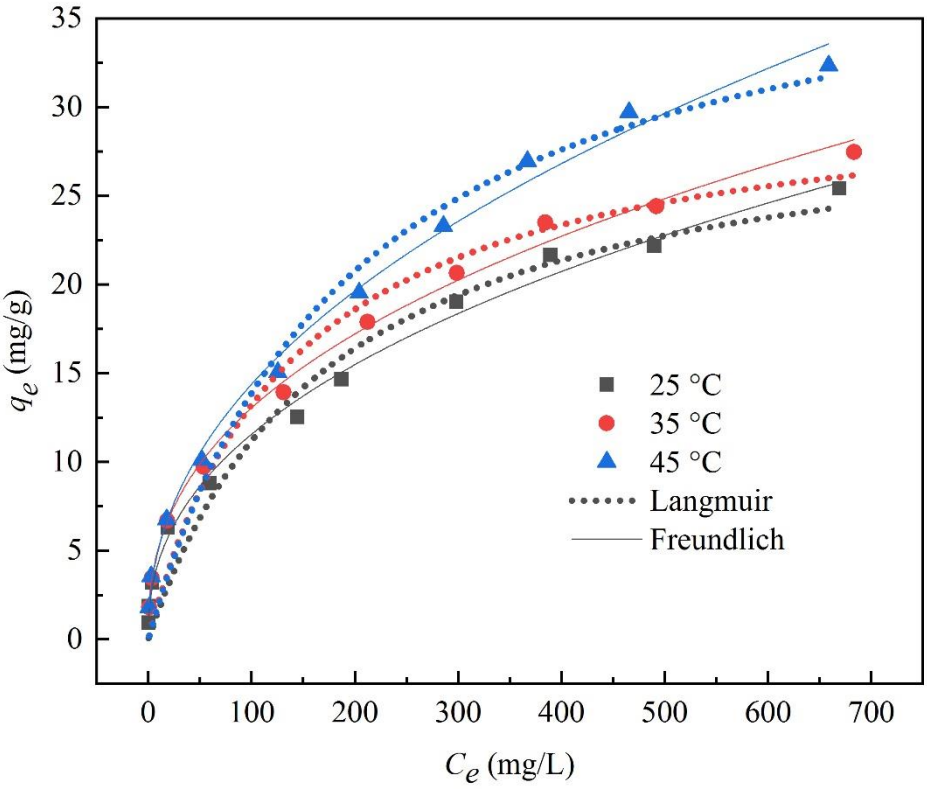

Figure 3-10. Adsorption isotherms data and fitted models of phosphate adsorption onto TS-LDHs (initial P concentration=5-800 mg P/L, adsorbent dosage=5 g/L)

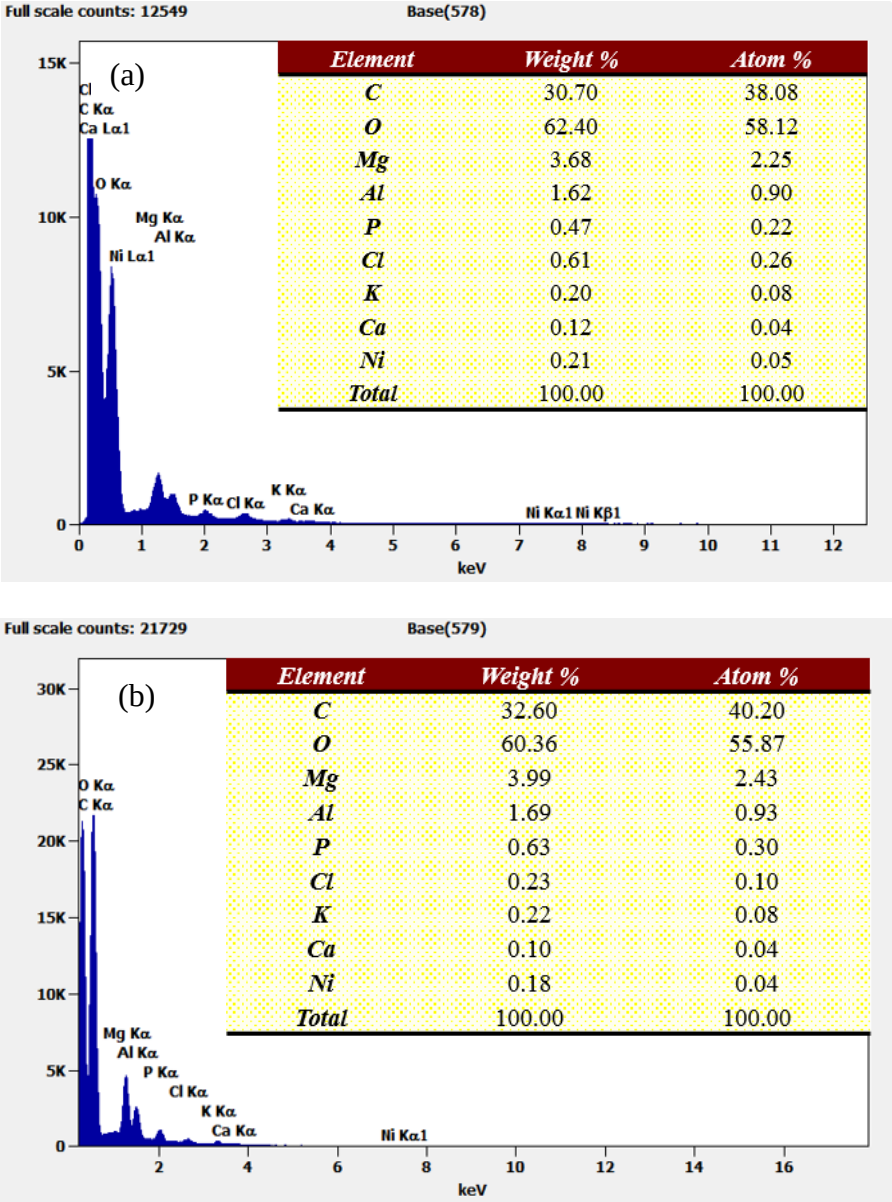

Figure 3-11. EDS spectra of TS-LDHs composite before (a) and after (b) phosphate adsorption.

Chapter 4 Potential application of carbon-based adsorbents derived from tobacco stalk

4.1 Background

Recent decades have witnessed that wastewater sludge production has enjoyed tremendous progress thanks to the improved municipal wastewater treatment along with an increasing growing amount of treated wastewater (Raheem et al., 2018). Wastewater treatment is able to produce great amount of sludge based on more than 90% water contents. It can be said that if there were no effective treatment and disposal methods, sludge would have been evolved to be a dramatic environmental threat (Wei et al., 2003). The treatment of sludge from conventional treatment is routinely built on high cost, taking up as much as 60% of the expense wastewater treatment plant (WWTP) operation (Niu et al., 2013). High-performance sludge dewatering procedures have been evolved to be an indispensable research area. Sludge treatment previous to disposal comprises a key aspect, which means the decrease of sludge volume in virtue of the separated solid from water (Qi et al., 2011).

Anaerobic digestion process, which is one of the major and essential part of many modern wastewater treatment plants (WWTP), is made up of four processes: hydrolysis, acidogenesis, acetogenesis as well methanogenesis. Following the four reaction phases, anaerobic digestion is able to perform the following function including lessening sludge amount, stabilizing organic fraction of sludge, killing pathogenic microorganisms, as well as producing renewable energy in the formality of methane in an effective way. However, under anaerobic conditions, polyphosphate and cations which up-taking by Phosphorus Accumulating Organisms are released, resulting in series of operating problems associated to the high phosphate concentrations in the reject water of the sludge dewatering. In addition, phosphate recycling from secondary resources, like sewage sludge, has been considered as a more sustainably strategy for phosphorus shortage issue (Cowie et al., 2015; Cao and Pawlowski, 2012). Therefore, efficient and applicable technologies for phosphate recovery from anaerobic digestion sludge need to be explored.

Potential supply shortages are in need of greater effective usage of P fertilizers on the basis of exploring new approaches to recycling the nutrient in the circumstances of agro-ecosystems (Kim et al., 2018). Various studies have proved that carbon-based materials after phosphate adsorption possessed the potential as phosphate-based fertilizer substitute. In addition, thermal

treatment, including pyrolysis and hydrothermal carbonization, could effectively convert biomass inherent P into bioavailable phosphate, which highlights the potential of biomass derived chars as a P-rich fertilizer for agricultural production (Kleemann et al., 2017; Grűbel et al., 2013). Apart from these, recent studies indicated the use of incorporating carbon-based material into agricultural soils as a soil amendment can provide additional benefits, such as improving soil fertility (Cowie et al., 2015), sequestering carbon (Woolf et al., 2010), encouraging the host of beneficial microorganism and reducing nitrate content in vegetation (Maroušek et al., 2018).

Based on above, this chapter aimed to explore the potential of agricultural and environmental applications for synthesized composite. On the one hand, the potential of P-loaded carbon-based adsorbents as phosphatic fertilizer were evaluated. On the other hand, the P removal capabilities and the sludge conditioning ability of synthesized carbon-based composite employed for anaerobically digested sludge treatment were compared.

4.2 Material and methods

4.2.1 Materials

An anaerobically digested (AD) sludge sample was obtained from the anaerobic digestion tank in the Shimodate WWTP in Chikusei, Ibaraki, Japan. The sludge sample was stored in 20 L polypropylene tanks at 4°C before experiment. The basic characteristics of obtained AD sludge were as follow: Total solids content: 8.92±0.11 g/L; Volatile solids content: 6.45± 0.15 g/L; pH: 7.75±0.02).

Carbon-based composite used in this chapter, were pristine biochar, $FeCl_3$-modified biochar, pristine hydrochar and Mg/Al-LDHs decorated hydrochar, which had synthesized in the previous two chapters.

4.2.2 Potential as phosphatic fertilizer

P fractionation of the pristine biochar, the $FeCl_3$-modified biochar, the pristine hydrochar, the Mg/Al-LDHs decorated hydrochar and the corresponding P-loaded composites which were gathered after kinetics study in chapters 3 and 4 were measured through the Standard Measurement and Test (SMT) procedure (Pardo et al 2004). According to the SMT procedure, Total Phosphorus (TP) could be grouped into organic phosphorus (OP) and inorganic phosphorus (IP), and IP could be further divided into apatite phosphorus (AP, calcium associated forms) and non-apatite inorganic phosphorus (NAIP, the fractions bound to the

oxides and hydroxides of Mn, Al and Fe) (Pardo et al 2004). Among them, OP and NAIP were to be found bioactive and potentially available for release and utilization, thus P bioavailability ((NAIP+OP)/TP) of the carbon-based composite could be evaluated based on the SMT program.

4.2.3 Sludge conditioning with carbon-based composite

Anaerobically digested sludge treatment experiments were performed in 15 mL centrifuge tubes to evaluate the performance of simultaneously phosphate removal capability and the sludge dewatering ability. For the effect of contact time, 0.2 g of samples were added into a series of test tubes containing 10 mL AD sludge for a certain time. For the effect of dosage, certain amount of samples (0.05, 0.1, 0.2, 0.3, 0.4, 0.5 g) were added into a series of test tubes containing 10 mL AD sludge, based on the results about the effect of contact time. Reaction time was fixed to 3 h. After above steps, the mixtures were shaken at room temperature (25±2 °C) under 50 rpm.

Capillary suction time (CST) was measured with a CST-1 meter (Central Kagaku Corp., Japan). The AD sludge was filtrated through 0.45 μm membrane filter and phosphate concentrations in the supernatants were detected with the ascorbic acid method (4500-P E) (APHA, 2012).

4.2.4 Metal leaching analysis

In order to identify the leachability of decorative metals from TS-Fe(Ⅲ) and TS-LDHs, batch experiments were conducted as follows: 0.1g samples were added into a series of centrifuge tubes containing 20 mL deionized water. The pH value was adjusted to a certain value (3, 5, 7, 9, 11 ± 0.05) by adding 0.01M HCl or NaOH. After 24 h shaking (100 rpm), the concentrations of Fe released from TS-Fe(Ⅲ) and Mg and Al leaching from TS-LDHs were detected by ICPS (Shimadzu ICPS-8100, Japan).

4.3 Results and discussion

4.3.1 Potential as phosphatic fertilizer

The P distribution of synthesized carbon-based composite is shown in Fig. 4-1. After thermal treatment, the amount of obtained biochar or hydrochar was decreased compared to the original biomass feedstock, resulting in the enrichment of phosphorus content per unit weight. In order to eliminate the interference of biomass weight reduction, the P fractionation was calculated based on the original weight of TS used in the pyrolysis or the hydrothermal

carbonization process. As for the raw TS, OP, NAIP and AP occupied 21.3%, 24.1% and 54.6% of TP, respectively, more than half of the P was difficult to decompose. After pyrolytic reaction, the NAIP of raw biochar and hydrochar almost disappeared, which could be explained by the potentially released feature of NAIP and could be recovered as the liquid fertilizer. After P adsorption, the TP of P-loaded $FeCl_3$-modified biochar and TS-LDHs were dramatically increased, while the NAIP proportions were increased to 36.8% and 54.2%. It's worth noting that, TS-LDHs before and after adsorption both possessed a high content of NAIP and AP (> 93%). The high content of bioavailable P (especially NAIP) contents reflected a high potential for being used as the P fertilizer.

4.3.2 Effect of contact time on AD sludge treatment

$FeCl_3$-modified biochar and TS-LDHs were employed for AD sludge conditioning and of excess phosphate removal. The effect of contact time on P removal was studied and results are represented in Fig. 4-2. TS-LDHs showed a higher P removal capacity than TS-Fe(Ⅲ), while TS-Fe(Ⅲ) exhibited a faster capture of P from AD sludge. 86% of the ultimate adsorption completed within the first 10 min on TS-Fe(Ⅲ) and 5 h were required for TS-LDHs to achieve a similar P depuration. A rapid phosphate adsorption was observed in the first 3h for TS-LDH (85%) and 1h for TS-Fe(Ⅲ) (91%). From a practical and economic viewpoint, the reaction time was fixed to 3h for the following experiments. The experimental data were fitted to pseudo first-order model and pseudo second-order model and the corresponding parameters are summarized. According to the correlation coefficients, the pseudo second-order model (R^2 > 0.95) simulated the process better than the pseudo first-order model. The result was consistent with the kinetic studies in chapters 2 and 3, further implying that the phosphate adsorption on the $FeCl_3$-modified biochar and the TS-LDHs might be controlled by the chemisorption process.

The effect of contact time on sludge dewatering ability was conducted, and results are represented in Fig.4-2. In general, CST was accepted as a parameter to determine the dewaterability of the sludge under laboratory conditions. TS-Fe(Ⅲ) showed much better dewatering ability than TS-LDHs. With the reaction time increasing, 54.1% - 62.3% of reduction percentage of CST were achieved by TS-Fe(Ⅲ), and the reduction percentage of CST decreased from 54.2% to 9.26% by TS-LDHs. It was suggested that TS-Fe(Ⅲ) could be a promising carbon-based composite for sludge dewatering enhancement.

4.3.3 Effect of dosage on AD sludge treatment

The P removal and the dewatering performance for AD sludge were carried out as a factor of TS-Fe(Ⅲ) and TS-LDHs dosage. As shown in Fig. 4-3, the P removal efficiency was increased obviously with the increase of dosage, and achieved 89.0% (on TS-Fe(Ⅲ)) and 77.5% (on TS-LDHs) P removal at dose of 5.52 g/g (based on TS of AD sludge), respectively. The reduction percentage of CST also exhibited an increasing trend with the increase of dosage, and TS-Fe(Ⅲ) showed higher reduction of CST than TS-LDHs. Overall, TS-Fe(Ⅲ) showed better performance on P removal and sludge dewaterability.

4.3.4 Metal leaching analysis

The concentrations of Fe released from $FeCl_3$-modified biochar were 0.020, 0.026, 0.019, 0.022, 0.075 mg/L, respectively, indicating ignorable dissolution of Fe and good stability of $FeCl_3$-modified biochar under different pH conditions. This result was consistent with previous report, in which a negligible dissolution of Fe from the pineapple peel biochar has been documented (Li et al., 2018a).

Equally, in the case of TS-LDHs, the contents of Al in the leachate were 0.09, 0.37, 0.26, 0.20, 1.05 mg/L, corresponding to different pH values. It can be found that the detachment of Al was affected by the pH conditions and more leaching Al was detected at the distilled water pH 11. However, the detachment of Al was undesirable when the distilled water pH value in the range of 3-10, and the actual pH conditions in the practical application were lower than 11. Unfortunately, high amount of free Mg (12.54, 9.32, 9.53, 9.25, 6.06 mg/L) have been detected under the different experimental pH conditions ranging from 3 to 11. The high dissolution of Mg may be caused by the relatively high content of Mg in the TS-LDHs comparing with combined Al. Considering a practical perspective, further improvement of the preparation of TS-LDHs was demanded, like reducing Mg content and replacing by another metal.

4.4 Summary

In this chapter, potential applications of carbon-based composite ($FeCl_3$-modified biochar and TS-LDHs) were evaluated on the respect of P-loaded carbon-based adsorbents as phosphatic fertilizer and simultaneously P elimination and AD sludge conditioning. Morever, the leachability of decorative metals was also studied to evaluate the side effect of $FeCl_3$-modified biochar and TS-LDHs employing in phosphate removal.

After adsorption, TS-Fe(Ⅲ) and TS-LDHs containing highly bioavailable P (especially NAIP) contents reflected a high potential for being used as the P fertilizer. However, considering the high content of NAIP and AP (> 93%) in TS-LDHs before and after adsorption, TS-LDHs were comparatively recommended as a potential phosphatic fertilizer substitute. For sludge treatment, after 24 h reaction, TS-LDHs showed a higher P removal capacity than TS-Fe(Ⅲ), while TS-Fe(Ⅲ) exhibited a faster capture of P. 54.1% - 62.3% of stable reduction percentage of CST and 89.0% P removal efficiency were achieved by TS-Fe(Ⅲ) when it was introduced to high phosphorus concentration AD sludge. In addition, $FeCl_3$-modified biochar showed a good stability under different pH conditions, whilst, Mg leaching potential may hinder the practical application of TS-LDHs, hence further improvement was claimed. The results of obvious enhancement of sludge dewaterability, P removal ability and good stability suggested that TS-Fe(Ⅲ) could be a promising carbon-based composite for the AD sludge treatment and possessing high potentials for practical P recycling applications.

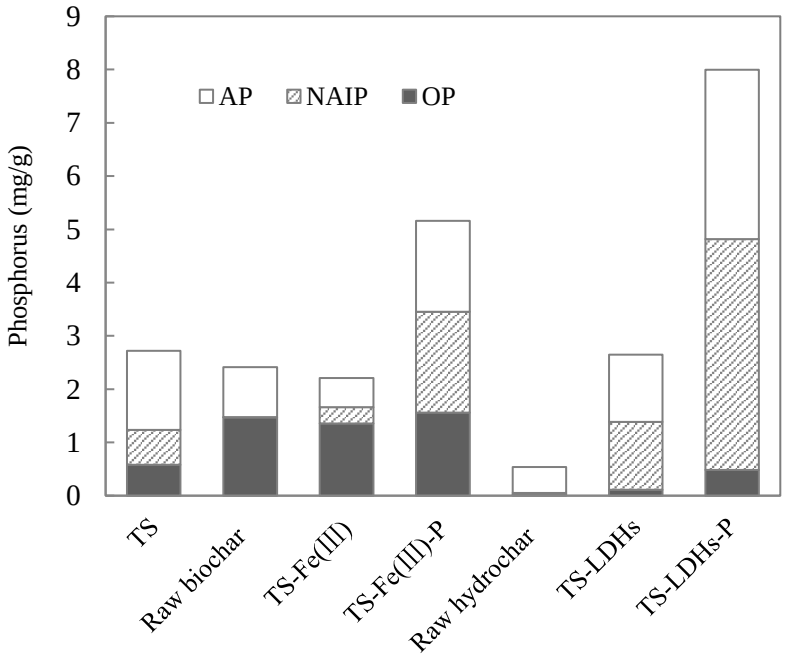

Figure 4-1. Phosphorus profiles (based on the original weight of TS).

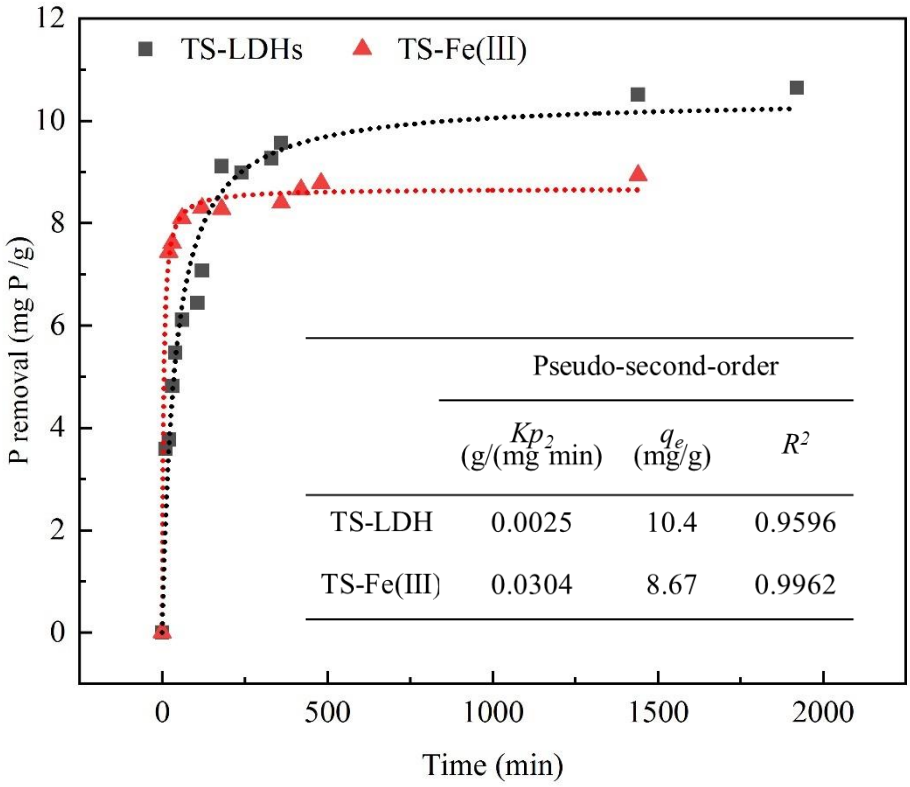

Figure 4-2. Adsorption kinetic curves. (Experimental conditions: 0.2 g TS-Fe(III) or TS-LDH, 10 mL AD sludge, initial P concentration: 274.62±5.76 mg/L, shaking speed: 50 rpm.)

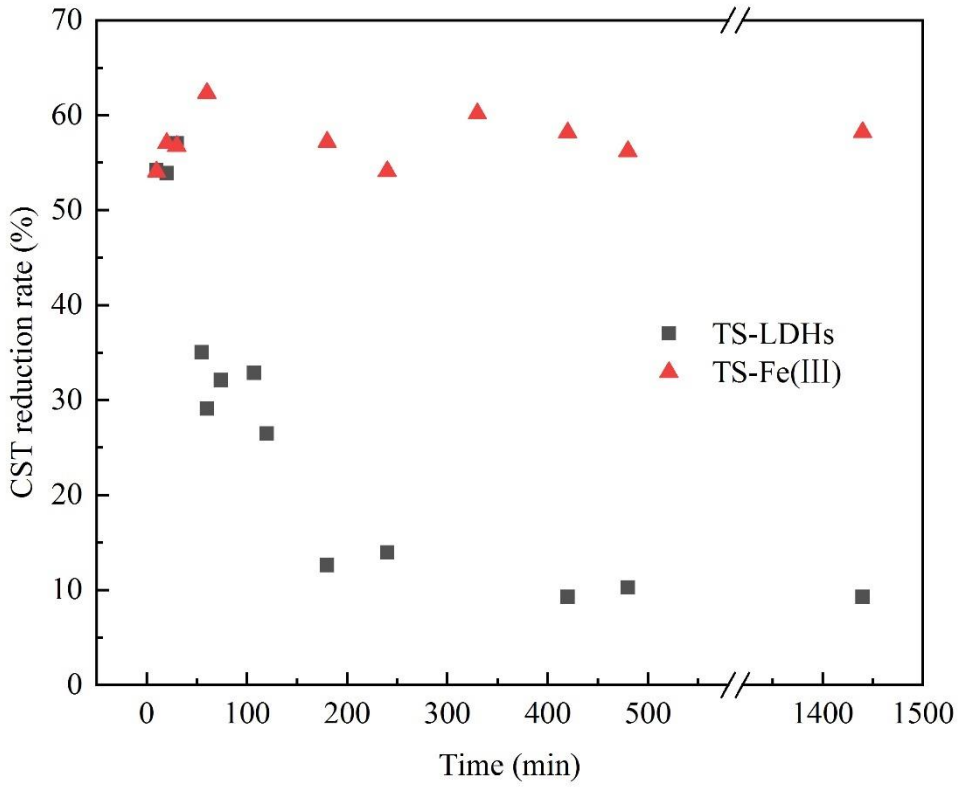

Figure 4-3. Effects of contact time on sludge dewaterability. (Experimental conditions: 0.2 g TS-Fe(III) or TS-LDH, 10 mL AD sludge, shaking speed: 50 rpm.)

(a)

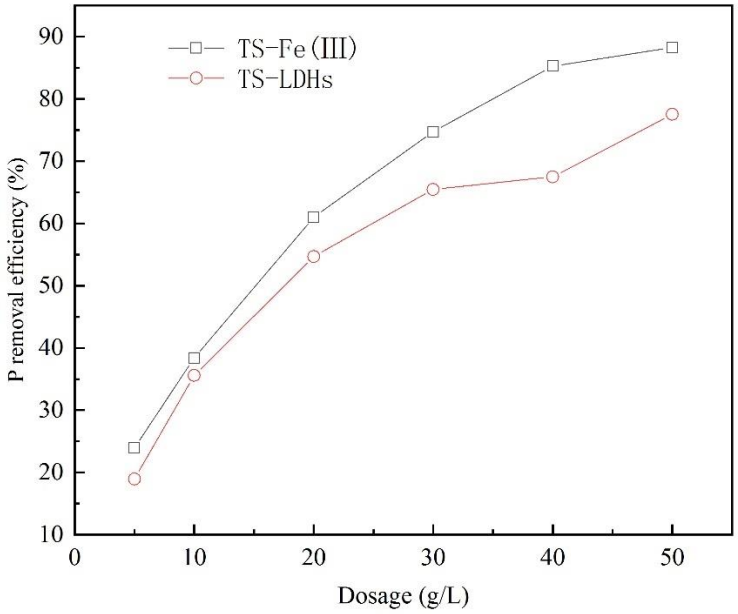

(b)

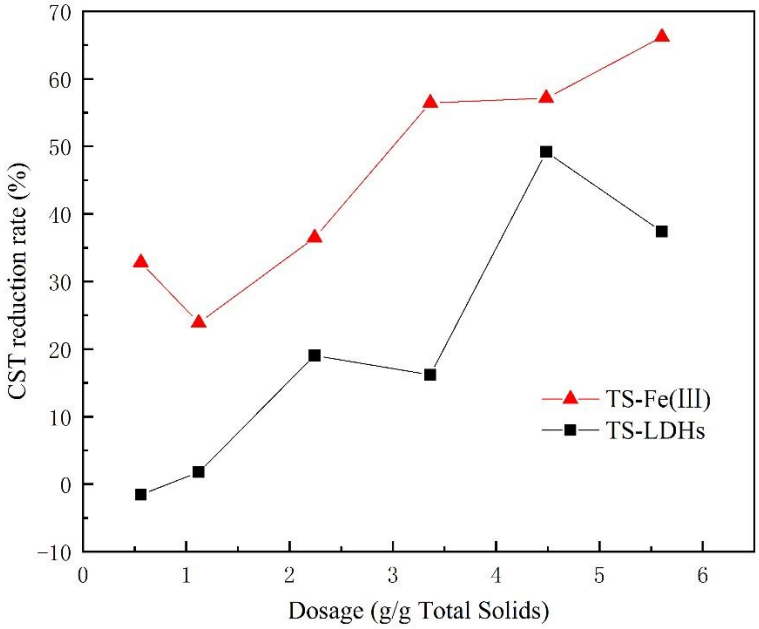

Figure 4-4. Effects of dosage on P removal (a) and sludge dewaterability (b). (Experimental conditions: 10 mL AD sludge, initial P concentration: 274.62±5.76 mg/L, shaking speed: 50 rpm, reaction time: 3 h.)

Chapter 5 Conclusions and future research

5.1 Conclusions

Exceeded phosphates presence in wastewater can cause eutrophication and have negatively effects on water bodies. Recycling of phosphorus from phosphate-rich wastewater could be a key strategy to prevent eutrophication and simultaneously solve the phosphorus shortage issue. In this study, low-cost adsorbents were prepared through hydrothermal carbonization or pyrolysis of agricultural waste (tobacco stalk) and can remove excessive phosphate from aquatic systems effectively, the involved mechanisms were interpreted and the potential applications of the novel carbon-based adsorbents were also evaluated. The main conclusions of this research could be summarized as follow:

(1) Three novel effective iron-modified biochars were prepared through the pyrolysis of waste TS and decorated by different ion modification. The maximum adsorption capacities of $FeCl_2$-modified, Fe^{2+}/Fe^{3+}-modified and $FeCl_3$-modified biochar calculated from Langmuir equation were 7.24 mg/g, 7.50 mg/g and 17.4 mg/g, respectively. $FeCl_3$-modified biochar exhibited a rapid and acid favorable phosphate removal, and the existence of other anions could hardly compete with phosphate species. The main mechanism involved should be proposed as ligand exchange and electrostatic attraction. In general, $FeCl_3$-modified biochar, with low-cost, good selectivity, and high adsorption capacity, could be an attractive adsorbent for phosphorus-rich wastewater remediation.

(2) Tobacco stalk was used for the hydrochar production and simultaneously modified by MgAl-LDHs through a one-step HTC method, using for the adsorption of phosphate. The adsorption results showed that TS-LDHs composites were very fast and efficient in phosphate adsorption in a wide pH range or under the coexistence of high level of competing anions. The maximum adsorption capacity acquired by the Langmuir model was up to 41.2 mg P/g at 45 °C, much higher than many adsorbents. The adsorption mechanisms involved are ion exchange, ligand exchange and electrostatic attraction. MgAl-LDHs decorated hydrochar composite could be a promising alternative of carbon-based adsorbent for phosphate removal from wastewater.

(3) For actual application, carbon-based adsorbents were employed for digested sludge treatment, 54.1% - 62.3% of stable reduction percentage of CST and 89.0% P removal efficiency were achieved by TS-Fe(Ⅲ). Obvious enhancement of sludge dewaterability

and P removal ability suggested that carbon-based adsorbents is proposed as a way for simultaneously phosphorus removal and sludge conditioning.

(4) For P utilization, after adsorption, TS-Fe(Ⅲ) and TS-LDHs containing highly bioavailable P (especially NAIP) contents reflected high potential for being used as P fertilizer, in which P can be retained in soils and having positive effects on the restoration of soil ecosystem and carbon sequestration.

5.2 Future perspectives

As a deficient nonrenewable resource, the critical role of P in agriculture and industry reclaimed P recovery from phosphate contaminated wastewater. As it has been reported in this study, carbon-based adsorbents derived from tobacco stalk, a typical agricultural waste, have been synthesized successfully and showed the ability for phosphate removal from aqueous solution, in addition, phosphorus recycling and reuse could be further realized by application of phosphate loaded carbon-based adsorbents as fertilizer in agriculture for food production. This multipurpose technology was beneficial to maintain agricultural sustainability, prevent P pollution and eutrophication, and alleviate P shortage issue. Hydrothermal carbonization and pyrolysis employing in this thesis were main approaches for biomass converting to value-added products, corresponding to hydrochar and biochar. One step HTC process could simultaneously accomplish carbonization and modification of abundant biomass, and simplify the production steps, however, the leachability of metal called for an improvement of this method to meet the requirements for practical applications. Iron modified biochar produced in this study possessed multiple features, such as effective P removal ability, good stability, potentials for simultaneously phosphorus recovery and sludge conditioning. In order to further economize production costs of engineered biochar adsorbents, microwave-assisted pyrolysis could be a future attempt to reduce the reaction time of carbonization process. Overall, the goals of carbon-based adsorbents development for P retrieve were consistent with the key issues of low cost, high phosphate affinity, good stability, easily available and P recycling possibility as fertilizer.

5.3 Future research

Future research will be emphasized on the following respects:

(1) The thermal treatment condition and surface modification method should be further investigated and optimized in order to find out the most cost-effective and efficient one for P recovery.

(2) More attempts should be developed on the respect of easy separation of adsorbents from wastewater. Energy consumption during thermal treatment should be assessed on the economic aspect.

(3) The fertilizer value and safety of P loaded adsorbents, e.g. metal leaching, should be further studied from agricultural aspect.

(4) The mechanism of conditioning approach in this study should be investigated.

References

Alatalo, S. M., Repo, E., Mäkilä, E., Salonen, J., Vakkilainen, E., Sillanpää, M. (2013). Adsorption behavior of hydrothermally treated municipal sludge and pulp and paper industry sludge. *Bioresource Technology*, *147*, 71–76.

Altmann, J., Sperlich, A., Jekel, M. (2015). Integrating organic micropollutant removal into tertiary filtration: Combining PAC adsorption with advanced phosphorus removal. *Water research*, *84*, 58-65.

Anirudhan, T. S., Noeline, B. F., Manohar, D. M. (2006). Phosphate removal from wastewaters using a weak anion exchanger prepared from a lignocellulosic residue. *Environmental Science and Technology*, *40*(8), 2740–2745.

APHA (American Public Health Association), 2012. Standard Methods for the Examination of Water and Wastewater, twenty-second ed. American Public Health Association, Washington DC.

Australian and New Zealand Environment and Conservation Council, and Agriculture and Resource Management Council of Australia and New Zealand, 2000. Australian and New Zealand Guidelines for Fresh and Marine Water Quality.

Barca, C., Gérente, C., Meyer, D., Chazarenc, F., Andrès, Y. (2012). Phosphate removal from synthetic and real wastewater using steel slags produced in Europe. *Water Research*, *46*(7), 2376-2384.

Biswas, B. K., Inoue, K., Ghimire, K. N., Harada, H., Ohto, K., Kawakita, H. (2008). Removal and recovery of phosphorus from water by means of adsorption onto orange waste gel loaded with zirconium. *Bioresource Technology*, *99*(18), 8685–8690.

Borggaard, O. K., Raben-Lange, B., Gimsing, A. L., Strobel, B. W. (2005). Influence of humic substances on phosphate adsorption by aluminium and iron oxides. *Geoderma*, *127*(3-4), 270-279.

Brix, H., Arias, C. A., Del Bubba, M. (2001). Media selection for sustainable phosphorus removal in subsurface flow constructed wetlands. *Water science and technology*, *44*(11-12), 47-54.

Bui, T. H., Hong, S. P., Yoon, J. (2018). Development of nanoscale zirconium molybdate embedded anion exchange resin for selective removal of phosphate. *Water Research*, *134*, 22-31.

Cai, R., Wang, X., Ji, X., Peng, B., Tan, C., Huang, X. (2017). Phosphate reclaim from simulated and real eutrophic water by magnetic biochar derived from water hyacinth. *Journal of Environmental Management*, *187*, 212–219.

Cao, Y., Pawłowski, A. (2012). Sewage sludge-to-energy approaches based on anaerobic digestion and pyrolysis: Brief overview and energy efficiency assessment. *Renewable and Sustainable Energy Reviews*, *16*(3), 1657-1665.

Case, S. D. C., Mcnamara, N. P., Reay, D. S., Whitaker, J. (2014). Can biochar reduce soil greenhouse gas emissions from a Miscanthus bioenergy crop? *GCB Bioenergy*, *6*(1), 76

Cha, J. S., Park, S. H., Jung, S. C., Ryu, C., Jeon, J. K., Shin, M. C., Park, Y. K. (2016). Production and utilization of biochar: a review. *Journal of Industrial and Engineering Chemistry*, *40*, 1-15.

Chen, B., Chen, Z., and Lv, S. (2011). A novel magnetic biochar efficiently sorbs organic pollutants and phosphate. *Bioresource technology*, *102*(2), 716-723.

Chen, L., Chen, X. L., Zhou, C. H., Yang, H. M., Ji, S. F., Tong, D. S., Chu, M. Q. (2017). Environmental-friendly montmorillonite-biochar composites: Facile production and tunable adsorption-release of ammonium and phosphate. *Journal of cleaner production*, *156*, 648-659.

Cowie, A., Woolf, D., Gaunt, J., Brandão, M., de la Rosa, R. A., Cowie, A. (2015). Biochar, carbon accounting and climate change. In *Biochar for Environmental Management* (pp. 795-826). Routledge.

Crittenden, J. C., Trussell, R. R., Hand, D. W., Howe, K. J., Tchobanoglous, G. (2005). Ion exchange. *Water Treatment Principles and Design. 2nd. Hoboken: John Wiley and Sons*, *16*, 1359-1428.

Dai, L., Wu, B., Tan, F., He, M., Wang, W., Qin, H., Hu, Q. (2014). Engineered hydrochar composites for phosphorus removal / recovery : Lanthanum doped hydrochar prepared by hydrothermal carbonization of lanthanum pretreated rice straw. *Bioresource Technology*, *161*, 327–332.

Das, J., Patra, B. S., Baliarsingh, N., Parida, K. M. (2006). Adsorption of phosphate by layered double hydroxides in aqueous solutions. *Applied Clay Science*, *32*(3-4), 252-260.

Desmidt, E., Ghyselbrecht, K., Zhang, Y., Pinoy, L., Van der Bruggen, B., Verstraete, W., Meesschaert, B. (2015). Global phosphorus scarcity and full-scale P-recovery techniques: a review. *Critical Reviews in Environmental Science and Technology*, *45*(4), 336-384.

Donnert, D., Salecker, M. (1999). Elimination of phosphorus from waste water by crystallization. *Environmental Technology*, *20*(7), 735-742.

Eljamal, O., Okawauchi, J., Hiramatsu, K., Harada, M. (2013). Phosphorus sorption from aqueous solution using natural materials. *Environmental Earth Sciences*, *68*(3), 859–863.

Elser, J. J. (2012). Phosphorus: a limiting nutrient for humanity? *Current Opinion in Biotechnology*, *23*(6), 833–838.

Environment Agency. (2000). Aquatic eutrophication in England and Wales: A management strategy.

European Commission. (2010). *Europe 2020 Flagship Initiative Innovation Union. Brussels, 6.10.2010 COM(2010) 546 final*. (2010).

Fang, J., Zhan, L., Ok, Y. S., Gao, B. (2018). Minireview of potential applications of hydrochar derived from hydrothermal carbonization of biomass. *Journal of Industrial and Engineering Chemistry*, *57*, 15-21.

Gao, G., Clare, A. S., Rose, C., Caldwell, G. S. (2017). Eutrophication and warming-driven green tides (Ulva rigida) are predicted to increase under future climate change scenarios. *Marine Pollution Bulletin*, *114*(1), 439–447.

Ghosh, R. K., Reddy, D. D. (2013). Tobacco stem ash as an adsorbent for removal of methylene blue from aqueous solution: equilibrium, kinetics, and mechanism of adsorption. *Water, Air, and Soil Pollution*, *224*(6), 1582.

Gnandi, K., Tchangbedji, G., Killi, K., Baba, G., Abbe, K. (2006). The impact of phosphate mine tailings on the bioaccumulation of heavy metals in marine fish and crustaceans from the coastal zone of Togo. *Mine Water and the Environment*, *25*(1), 56–62.

Goh, K. H., Lim, T. T., Dong, Z. (2008). Application of layered double hydroxides for removal of oxyanions: a review. *Water Research*, *42*(6-7), 1343-1368.

Grűbel, K., Machnicka, A., Wacławek, S. (2013). Impact of alkalization of surplus activated sludge on biogas production. *Ecological Chemistry and Engineering S*, *20*(2), 343-351.

Guo, S., Dong, X., Zhu, C., Han, Y., Ma, F., Wu, T. (2017). Pyrolysis behaviors and thermodynamics properties of hydrochar from bamboo (Phyllostachys heterocycla cv. pubescens) shoot shell. *Bioresource Technology*, *233*, 92-98.

Gutierrez, O., Park, D., Sharma, K. R., Yuan, Z. (2010). Iron salts dosage for sulfide control in sewers induces chemical phosphorus removal during wastewater treatment. *Water Research*, *44*(11), 3467–3475.

Halajnia, A., Oustan, S., Najafi, N., Khataee, A. R., and Lakzian, A. (2013). Adsorption–desorption characteristics of nitrate, phosphate and sulfate on Mg–Al layered double hydroxide. *Applied Clay Science*, *80*, 305-312.

Hansen, A. M., Hernández-Martínez, C., Falcón-Rojas, A. (2017). Evaluation of Eutrophication Control Through Hypolimnetic Oxygenation. *Procedia Earth and Planetary Science*, *17*, 598–601.

He, R., Peng, Z., Lyu, H., Huang, H., Nan, Q., Tang, J. (2018). Synthesis and characterization of an iron-impregnated biochar for aqueous arsenic removal. *Science of the Total Environment*, *612*, 1177-1186.

Huang, H., Liu, J., Zhang, P., Zhang, D., Gao, F. (2017a). Investigation on the simultaneous removal of fluoride, ammonia nitrogen and phosphate from semiconductor wastewater using chemical precipitation. *Chemical Engineering Journal*, *307*, 696–706.

Huang, H., Zhang, P., Zhang, Z., Liu, J., Xiao, J., Gao, F. (2016). Simultaneous removal of ammonia nitrogen and recovery of phosphate from swine wastewater by struvite electrochemical precipitation and recycling technology. *Journal of Cleaner Production*, *127*, 302-310.

Huang, W., Zhang, Y., Li, D. (2017b). Adsorptive removal of phosphate from water using mesoporous materials: A review. *Journal of Environmental Management*, *193*, 470–482.

Huang, Y., Lee, X., Grattieri, M., Yuan, M., Cai, R., Macazo, F. C., Minteer, S. D. (2020). Modified biochar for phosphate adsorption in environmentally relevant conditions. *Chemical Engineering Journal*, *380*, 122375.

Hug, S. J., Canonica, L., Wegelin, M., Gechter, D., Von Gunten, U. (2001). Solar oxidation and removal of arsenic at circumneutral pH in iron containing waters. *Environmental Science and Technology*, *35*(10), 2114-2121.

Ismail, Z. Z. (2012). Kinetic study for phosphate removal from water by recycled date-palm wastes as agricultural by-products. *International Journal of Environmental Studies*, *69*(1), 135-149.

Jack, J., Huggins, T. M., Huang, Y., Fang, Y., Ren, Z. J. (2019). Production of magnetic biochar from waste-derived fungal biomass for phosphorus removal and recovery. *Journal of Cleaner Production*, *224*, 100–106.

Jiang, D., Chu, B., Amano, Y., Machida, M. (2018). Removal and recovery of phosphate from water by Mg-laden biochar: Batch and column studies. *Colloids and Surfaces A: Physicochemical and Engineering Aspects*, *558*, 429-437.

Jung, K. W., Hwang, M. J., Ahn, K. H., Ok, Y. S. (2015a). Kinetic study on phosphate removal from aqueous solution by biochar derived from peanut shell as renewable adsorptive media. *International Journal of Environmental Science and Technology*, *12*(10), 3363–3372.

Jung, Kyung Won, Hwang, M. J., Jeong, T. U., Ahn, K. H. (2015b). A novel approach for preparation of modified-biochar derived from marine macroalgae: Dual purpose electro-modification for improvement of surface area and metal impregnation. *Bioresource Technology*, *191*, 342–345.

Jung, Kyung Won, Kim, K., Jeong, T. U., Ahn, K. H. (2016). Influence of pyrolysis temperature on characteristics and phosphate adsorption capability of biochar derived from waste-marine macroalgae (Undaria pinnatifida roots). *Bioresource Technology*, *200*, 1024–1028.

Karageorgiou, K., Paschalis, M., Anastassakis, G. N. (2007). Removal of phosphate species from solution by adsorption onto calcite used as natural adsorbent. *Journal of Hazardous Materials*, *139*(3), 447-452.

Karthikeyan, K. G., Tshabalala, M. A., Wang, D. (2002). Use of lignocellulose materials as sorption media for phosphorus removal. In *[2002 ASAE annual international meeting: CIGR XVth World Congress: Chicago, Illinois, USA, July 28-July 31, 2002. St. Joseph, MI: ASAE, 2002]: 15 pages.*.

Kim, E. H., Lee, D. W., Hwang, H. K., Yim, S. (2006). Recovery of phosphates from wastewater using converter slag: Kinetics analysis of a completely mixed phosphorus crystallization process. *Chemosphere*, *63*(2), 192-201.

Kim, J. A., Vijayaraghavan, K., Reddy, D. H. K., Yun, Y. S. (2018). A phosphorus-enriched biochar fertilizer from bio-fermentation waste: a potential alternative source for phosphorus fertilizers. *Journal of Cleaner Production*, *196*, 163-171.

Kleemann, R., Chenoweth, J., Clift, R., Morse, S., Pearce, P., Saroj, D. (2017). Comparison of phosphorus recovery from incinerated sewage sludge ash (ISSA) and pyrolysed sewage sludge char (PSSC). *Waste Management*, *60*, 201-210.

Krishnan, K. A., Haridas, A. (2008). Removal of phosphate from aqueous solutions and sewage using natural and surface modified coir pith. *Journal of Hazardous Materials*, *152*(2), 527–535.

Kumar, P., Sudha, S., Chand, S., Srivastava, V. C. (2010). Phosphate removal from aqueous solution using coir-pith activated carbon. *Separation Science and Technology*, *45*(10), 1463-1470.

Kuzawa, K., Jung, Y. J., Kiso, Y., Yamada, T., Nagai, M., Lee, T. G. (2006). Phosphate removal and recovery with a synthetic hydrotalcite as an adsorbent. *Chemosphere*, *62*(1), 45-52.

Lalley, J., Han, C., Li, X., Dionysiou, D. D., Nadagouda, M. N. (2016). Phosphate adsorption using modified iron oxide-based sorbents in lake water: Kinetics, equilibrium, and column tests. *Chemical Engineering Journal*, *284*, 1386–1396.

Lee, J., Rai, P. K., Jeon, Y. J., Kim, K. H., Kwon, E. E. (2017). The role of algae and cyanobacteria in the production and release of odorants in water. *Environmental Pollution*, *227*, 252–262.

Li, M., Liu, J., Xu, Y., Qian, G. (2016a). Phosphate adsorption on metal oxides and metal hydroxides: A comparative review. *Environmental Reviews*, *24*(3), 319-332.

Li, R., Wang, J. J., Zhou, B., Awasthi, M. K., Ali, A., Zhang, Z., Mahar, A. (2016b). Enhancing phosphate adsorption by Mg/Al layered double hydroxide functionalized biochar with different Mg/Al ratios. *Science of the Total Environment*, *559*, 121–129.

Li, R., Wang, J. J., Zhou, B., Awasthi, M. K., Ali, A., Zhang, Z., Mahar, A. (2016c). Recovery of phosphate from aqueous solution by magnesium oxide decorated magnetic biochar and its potential as phosphate-based fertilizer substitute. *Bioresource Technology*, *215*, 209–214.

Li, T., Su, X., Yu, X., Song, H., Zhu, Y., Zhang, Y. (2018). La $(OH)_3$-modified magnetic pineapple biochar as novel adsorbents for efficient phosphate removal. *Bioresource Technology*, *263*, 207-213.

Li, W., Zhang, L., Peng, J., Li, N., Zhang, S., Guo, S. (2008). Tobacco stems as a low cost adsorbent for the removal of Pb (II) from wastewater: Equilibrium and kinetic studies. *Industrial Crops and Products*, *28*(3), 294-302.

Li, Y., Meas, A., Shan, S., Yang, R., Gai, X., Wang, H., Tsend, N. (2018). Hydrochars from bamboo sawdust through acid assisted and two-stage hydrothermal carbonization for removal of two organics from aqueous solution. *Bioresource Technology*, *261*, 257-264.

Liberti, L., Boari, G., Passino, R. (1979). Phosphates and ammonia recovery from secondary effluents by selective ion exchange with production of a slow-release fertilizer. *Water Research*, *13*(1), 65–73.

Lin, Y., Yan, W., Sheng, K. (2016). Effect of pyrolysis conditions on the characteristics of biochar produced from a tobacco stem. *Waste Management and Research*, *34*(8), 793-801.

Liu, J., Zhou, Q., Chen, J., Zhang, L., Chang, N. (2013). Phosphate adsorption on hydroxyl-iron-lanthanum doped activated carbon fiber. *Chemical Engineering Journal*, *215–216*, 859–867.

Liu, R., Chi, L., Wang, X., Sui, Y., Wang, Y., Arandiyan, H. (2018). Review of metal (hydr) oxide and other adsorptive materials for phosphate removal from water. *Journal of Environmental Chemical Engineering*, *6*(4), 5269–5286.

Long, F., Gong, J. L., Zeng, G. M., Chen, L., Wang, X. Y., Deng, J. H., Zhang, X. R. (2011). Removal of phosphate from aqueous solution by magnetic Fe–Zr binary oxide. *Chemical Engineering Journal*, *171*(2), 448-455.

Lǔ, J., Liu, H., Liu, R., Zhao, X., Sun, L., Qu, J. (2013). Adsorptive removal of phosphate by a nanostructured Fe–Al–Mn trimetal oxide adsorbent. *Powder Technology*, *233*, 146-154.

Lu, N. C., Liu, J. C. (2010). Removal of phosphate and fluoride from wastewater by a hybrid precipitation-microfiltration process. *Separation and Purification Technology*, *74*(3), 329–335.

Lu, S. G., Bai, S. Q., Zhu, L., Shan, H. D. (2009). Removal mechanism of phosphate from aqueous solution by fly ash. *Journal of Hazardous Materials*, *161*(1), 95-101.

Maroušek, J., Kolář, L., Vochozka, M., Stehel, V., Maroušková, A. (2018). Biochar reduces nitrate level in red beet. *Environmental Science and Pollution Research*, *25*(18), 18200-18203.

Méndez, A., Gascó, G., Ruiz, B., Fuente, E. (2019). Hydrochars from industrial macroalgae "Gelidium Sesquipedale" biomass wastes. *Bioresource Technology*, *275*, 386-393.

Micháleková-Richveisová, B., Frišták, V., Pipíška, M., Ďuriška, L., Moreno-Jimenez, E., and Soja, G. (2017). Iron-impregnated biochars as effective phosphate sorption materials. *Environmental Science and Pollution Research*, *24*(1), 463-475.

Ministry of Environmental Protection, China (MEP), Discharge standard of pollutants for municipal wastewater treatment plant, Beijing, China, 2002.

Ministry of the environment, Government of Japan. (2003). Environmental Quality Standards

Mohan, D., Sarswat, A., Ok, Y. S., Pittman, C. U. (2014). Organic and inorganic contaminants removal from water with biochar, a renewable, low cost and sustainable adsorbent - A critical review. *Bioresource Technology*, *160*, 191–202.

Morse, G. K., Brett, S. W., Guy, J. A., Lester, J. N. (1998). Review: Phosphorus removal and recovery technologies. *Science of the Total Environment*, *212*(1), 69–81.

Mudyawabikwa, B., Mungondori, H. H., Tichagwa, L., Katwire, D. M. (2017). Methylene blue removal using a low-cost activated carbon adsorbent from tobacco stems: kinetic and equilibrium studies. *Water Science and Technology, 75*(10), 2390-2402.

Muhammad, A., Soares, A., Jefferson, B. (2019). The impact of background wastewater constituents on the selectivity and capacity of a hybrid ion exchange resin for phosphorus removal from wastewater. *Chemosphere, 224*, 494-501.

Neethling, J. B., Falk, M. W., Reardon, D. J., Clark, D. L., Pramanik, A. (2011). WERF Nutrient Challenge–Nutrient Regulations, Treatment Performance, and Sustainability Collide. *Proceedings of the Water Environment Federation, 2011*(18), 1-16.

Nguyen, T. A. H., Ngo, H. H., Guo, W. S., Zhang, J., Liang, S., Lee, D. J., Bui, X. T. (2014). Modification of agricultural waste/by-products for enhanced phosphate removal and recovery: potential and obstacles. *Bioresource technology, 169*, 750-762.

Niu, M., Zhang, W., Wang, D., Chen, Y., Chen, R. (2013). Correlation of physicochemical properties and sludge dewaterability under chemical conditioning using inorganic coagulants. *Bioresource Technology*, *144*, 337-343.

Novak, J. M., Cantrell, K. B., Watts, D. W. (2013). Compositional and thermal evaluation of lignocellulosic and poultry litter chars via high and low temperature pyrolysis. *BioEnergy Research*, *6*(1), 114-130.

Pardo, P., Rauret, G., López-Sánchez, J. F. (2004). Shortened screening method for phosphorus fractionation in sediments: a complementary approach to the standards, measurements and testing harmonised protocol. *Analytica Chimica Acta*, *508*(2), 201-206.

Park, J. H., Ok, Y. S., Kim, S. H., Cho, J. S., Heo, J. S., Delaune, R. D., Seo, D. C. (2015). Evaluation of phosphorus adsorption capacity of sesame straw biochar on aqueous solution: influence of activation methods and pyrolysis temperatures. *Environmental Geochemistry and Health*, *37*(6), 969–983.

Park, J. H., Ok, Y. S., Kim, S. H., Cho, J. S., Heo, J. S., Delaune, R. D., Seo, D. C. (2016). Competitive adsorption of heavy metals onto sesame straw biochar in aqueous solutions. *Chemosphere*, *142*, 77-83.

Peng, L., Dai, H., Wu, Y., Peng, Y., Lu, X. (2018). A comprehensive review of phosphorus recovery from wastewater by crystallization processes. *Chemosphere, 197*, 768-781.

Pratt, C., Parsons, S. A., Soares, A., Martin, B. D. (2012). Biologically and chemically mediated adsorption and precipitation of phosphorus from wastewater. *Current Opinion in Biotechnology*, *23*(6), 890-896.

Qi, Y., Thapa, K. B., Hoadley, A. F. (2011). Application of filtration aids for improving sludge dewatering properties–a review. *Chemical Engineering Journal*, *171*(2), 373-384.

Qiu, B., and Duan, F. (2019). Synthesis of industrial solid wastes/biochar composites and their use for adsorption of phosphate: From surface properties to sorption mechanism. *Colloids and Surfaces A: Physicochemical and Engineering Aspects*, *571*, 86-93.

Qiu, B., Duan, F. (2019). Synthesis of industrial solid wastes/biochar composites and their use for adsorption of phosphate: From surface properties to sorption mechanism. *Colloids and Surfaces A: Physicochemical and Engineering Aspects*, *571*, 86–93.

Raheem, A., Sikarwar, V. S., He, J., Dastyar, W., Dionysiou, D. D., Wang, W., Zhao, M. (2018). Opportunities and challenges in sustainable treatment and resource reuse of sewage sludge: a review. *Chemical Engineering Journal*, *337*, 616-641.

Reijnders, L. (2014). Phosphorus resources, their depletion and conservation, a review. *Resources, Conservation and Recycling*, *93*, 32–49.

Ren, J., Li, N., Li, L., An, J. K., Zhao, L., Ren, N. Q. (2015). Granulation and ferric oxides loading enable biochar derived from cotton stalk to remove phosphate from water. *Bioresource technology*, *178*, 119-125.

Riahi, K., Chaabane, S., Thayer, B. B. (2017). A kinetic modeling study of phosphate adsorption onto Phoenix dactylifera L. date palm fibers in batch mode. *Journal of Saudi Chemical Society*, *21*, S143-S152.

Ribas, M. C., Adebayo, M. A., Prola, L. D., Lima, E. C., Cataluña, R., Feris, L. A., ... and Calvete, T. (2014). Comparison of a homemade cocoa shell activated carbon with commercial activated carbon for the removal of reactive violet 5 dye from aqueous solutions. *Chemical Engineering Journal*, *248*, 315-326.

Rittmann, B. E., Mayer, B., Westerhoff, P., Edwards, M. (2011). Capturing the lost phosphorus. *Chemosphere*, *84*(6), 846-853.

Seida, Y., Nakano, Y. (2002). Removal of phosphate by layered double hydroxides containing iron. *Water Research*, *36*(5), 1306-1312.

Shi, W., Fu, Y., Jiang, W., Ye, Y., Kang, J., Liu, D., Xu, Z. (2019). Enhanced phosphate removal by zeolite loaded with Mg–Al–La ternary (hydr) oxides from aqueous solutions: performance and mechanism. *Chemical Engineering Journal*, *357*, 33-44.

Shih, Y. J., Abarca, R. R. M., de Luna, M. D. G., Huang, Y. H., Lu, M. C. (2017). Recovery of phosphorus from synthetic wastewaters by struvite crystallization in a fluidized-bed

reactor: effects of pH, phosphate concentration and coexisting ions. *Chemosphere*, *173*, 466-473.

Song, Y., Weidler, P. G., Berg, U., Nüesch, R., Donnert, D. (2006). Calcite-seeded crystallization of calcium phosphate for phosphorus recovery. *Chemosphere*, *63*(2), 236-243.

Sun, L., Wang, Z., Wei, X., Li, P., Zhang, H., Li, M., Wang, S. (2015). Enhanced biological nitrogen and phosphorus removal using sequencing batch membrane-aerated biofilm reactor. *Chemical Engineering Science*, *135*, 559-565.

Takaya, C. A., Fletcher, L. A., Singh, S., Okwuosa, U. C., Ross, A. B. (2016). Recovery of phosphate with chemically modified biochars. *Journal of Environmental Chemical Engineering*, *4*(1), 1156–1165.

Tan, K. L., Hameed, B. H. (2017). Insight into the adsorption kinetics models for the removal of contaminants from aqueous solutions. *Journal of the Taiwan Institute of Chemical Engineers*, *74*, 25-48.

Tofik, A. S., Taddesse, A. M., Tesfahun, K. T., Girma, G. G. (2016). Fe–Al binary oxide nanosorbent: synthesis, characterization and phosphate sorption property. *Journal of Environmental Chemical Engineering*, *4*(2), 2458-2468.

Trazzi, P. A., Leahy, J. J., Hayes, M. H., Kwapinski, W. (2016). Adsorption and desorption of phosphate on biochars. *Journal of Environmental Chemical Engineering*, *4*(1), 37-46.

Vikrant, K., Kim, K. H., Ok, Y. S., Tsang, D. C., Tsang, Y. F., Giri, B. S., Singh, R. S. (2018). Engineered/designer biochar for the removal of phosphate in water and wastewater. *Science of the Total Environment*, *616*, 1242-1260.

Wan, S., Wang, S., Li, Y., Gao, B. (2017). Functionalizing biochar with Mg–Al and Mg–Fe layered double hydroxides for removal of phosphate from aqueous solutions. *Journal of Industrial and Engineering Chemistry*, *47*, 246-253.

Wang, L., Wang, J., He, C., Lyu, W., Zhang, W., Yan, W., Yang, L. (2019). Development of rare earth element doped magnetic biochars with enhanced phosphate adsorption performance. *Colloids and Surfaces A: Physicochemical and Engineering Aspects*, *561*(September 2018), 236–243.

Wang, S., Kong, L., Long, J., Su, M., Diao, Z., Chang, X., Shih, K. (2018). Adsorption of phosphorus by calcium-flour biochar: Isotherm, kinetic and transformation studies. *Chemosphere*, *195*, 666–672.

Wang, Y., Zhang, F., Xu, S., Wang, X., Evans, D. G., Duan, X. (2008). Preparation of layered double hydroxide microspheres by spray drying. *Industrial & Engineering Chemistry Research*, *47*(15), 5746-5750.

Wang, Z., Lin, Y., Wu, D., Kong, H. (2016). Hydrous iron oxide modified diatomite as an active filtration medium for phosphate capture. *Chemosphere*, *144*, 1290–1298.

Wang, Z., Nie, E., Li, J., Yang, M., Zhao, Y., Luo, X., Zheng, Z. (2012). Equilibrium and kinetics of adsorption of phosphate onto iron-doped activated carbon. *Environmental Science and Pollution Research*, *19*(7), 2908-2917.

Wei, D., Li, B., Huang, H., Luo, L., Zhang, J., Yang, Y., Zhou, Y. (2018). Biochar-based functional materials in the purification of agricultural wastewater: fabrication, application and future research needs. *Chemosphere*, *197*, 165-180.

Wei, Y., van Houten, R. T., Borger, A. R., Eikelboom, D. H., Fan, Y. (2003). Comparison performances of membrane bioreactor and conventional activated sludge processes on sludge reduction induced by Oligochaete. *Environmental Science and Technology*, *37*(14), 3171-3180.

Woolf, D., Amonette, J. E., Street-Perrott, F. A., Lehmann, J., Joseph, S. (2010). Sustainable biochar to mitigate global climate change. *Nature Communications*, *1*, 56.

Xia, X., Liu, H., Shi, L., He, Y. (2012). *Tobacco Stem-Based Activated Carbons for High Performance Supercapacitors*. *21*(September), 1956–1961.

Xu, X., Gao, B., Yue, Q., Zhong, Q. (2011). Sorption of phosphate onto giant reed based adsorbent: FTIR, Raman spectrum analysis and dynamic sorption/desorption properties in filter bed. *Bioresource Technology*, *102*(9), 5278–5282.

Yadav, D., Kapur, M., Kumar, P., Mondal, M. K. (2015). Adsorptive removal of phosphate from aqueous solution using rice husk and fruit juice residue. *Process Safety and Environmental Protection*, *94*, 402-409.

Yan, L. G., Yang, K., Shan, R. R., Yan, T., Wei, J., Yu, S. J., Du, B. (2015). Kinetic, isotherm and thermodynamic investigations of phosphate adsorption onto core–shell Fe_3O_4@ LDHs composites with easy magnetic separation assistance. *Journal of Colloid and Interface Science*, *448*, 508-516.

Yang, K., Yan, L. G., Yang, Y. M., Yu, S. J., Shan, R. R., Yu, H. Q., Du, B. (2014). Adsorptive removal of phosphate by Mg–Al and Zn–Al layered double hydroxides: kinetics, isotherms and mechanisms. *Separation and Purification Technology*, *124*, 36-42.

Yao, Y., Gao, B., Inyang, M., Zimmerman, A. R., Cao, X., Pullammanappallil, P.,Yang, L. (2011). Biochar derived from anaerobically digested sugar beet tailings: characterization and phosphate removal potential. *Bioresource Technology*, *102*(10), 6273-6278.

Yi, H., Deng, H., Yang, L., Tang, X. L., Yu, Q., Ye, Z. (2013). Preparation of activated carbons from tobacco stems by potassium hydroxide activation and phosphine adsorption. *Separation Science and Technology*, *48*(5), 813-819.

Yin, Q., Ren, H., Wang, R., Zhao, Z. (2018a). Evaluation of nitrate and phosphate adsorption on Al-modified biochar: Influence of Al content. *Science of the Total Environment, 631–632*, 895–903.

Yin, Q., Wang, R., Zhao, Z. (2018b). Application of Mg–Al-modified biochar for simultaneous removal of ammonium, nitrate, and phosphate from eutrophic water. *Journal of Cleaner Production, 176*, 230–240.

Yuan, Z., Pratt, S., Batstone, D. J. (2012). Phosphorus recovery from wastewater through microbial processes. *Current Opinion in Biotechnology*, *23*(6), 878–883.

Zhang, H., Chen, C., Gray, E. M., Boyd, S. E., Yang, H., Zhang, D. (2016). Roles of biochar in improving phosphorus availability in soils: a phosphate adsorbent and a source of available phosphorus. *Geoderma*, *276*, 1-6.

Zhang, X., Fu, W., Yin, Y., Chen, Z., Qiu, R., Simonnot, M. O., Wang, X. (2018). Adsorption-reduction removal of Cr(VI) by tobacco petiole pyrolytic biochar: Batch experiment, kinetic and mechanism studies. *Bioresource Technology*, *268*, 149-157.

Zhang, Z., Yan, L., Yu, H., Yan, T., Li, X. (2019). Adsorption of phosphate from aqueous solution by vegetable biochar/layered double oxides: Fast removal and mechanistic studies. *Bioresource Technology*, *284*, 65-71.

Zhou, H., Jiang, Z., Wei, S. (2013). A novel absorbent of nano-Fe loaded biomass char and its enhanced adsorption capacity for phosphate in water. *Journal of Chemistry*, *2013*.

Zhu, Z., Huang, C. P., Zhu, Y., Wei, W., Qin, H. (2018). A hierarchical porous adsorbent of nano-α-Fe_2O_3/Fe_3O_4 on bamboo biochar (HPA-Fe/C-B) for the removal of phosphate from water. *Journal of Water Process Engineering*, *25*, 96–104.

Zoltek Jr, J. (1974). Phosphorus removal by orthophosphate nucleation. *Journal (Water Pollution Control Federation)*, 2498-2520.

Acknowledgements

My deepest gratitude goes first and foremost to my supervisor, Professor Zhenya Zhang, for his illuminating guidance about my study, constant encouragement to my spirit and genial friendship with all of us. It is not only his abundant knowledge and rigorous academic attitude but also his valuable character, like professionalism and seriousness, benefit me a lot, which I should follow in my future career.

Second, I would like to express my heartfelt gratitude to Associate Professor Zhongfang Lei, who has walked me through all the stages of the writing of this thesis. I am greatly indebted to Associate Professor Kazuya Shimizu, who have instructed and helped me a lot in the past three years. I also would like to express my great appreciation to another dissertation committee members, Associate Professor Motoo Utsumi, for his numerous willingness, suggestions, comments, and helpful discussions to serve as my advisory committee members.

I also owe my sincere gratitude to my fellow students and friends who gave me their help and time in listening to me and helping me overcome difficulties to accomplish this thesis, they are Dr. Ying Wang, Dr. Yong Jiang, Dr. Xi Yang, Dr. Tian Yuan, Dr. Yanfei Cheng, Dr. Nan Zhang, Dr. Qili Hu, Miss Qian Wang, Miss Xiaojing Yang, Miss Dirui Zhu, Mr. Chen Shi, Mr. Qingyue Shen, Mr. Yujie Fan, Mr. Xuezhi Wang, Mr. Zitao Guo, and Mr Yingxing Wang.

Last, I wish to express my appreciation to my beloved family for their loving considerations and great confidence in me all the time. This dissertation would not have been completed without their countless love and strong support.

Publications

1. He, H., Zhang, N., Chen, N., Lei, Z., Shimizu, K., and Zhang, Z. (2019). Efficient phosphate removal from wastewater by MgAl-LDHs modified hydrochar derived from tobacco stalk. *Bioresource Technology Reports*, *8*, 100348.
2. Wang, Y., He, H., Zhang, N., Shimizu, K., Lei, Z., and Zhang, Z. (2018). Efficient capture of phosphate from aqueous solution using acid activated akadama clay and mechanisms analysis. *Water Science and Technology*, *78*(7), 1603-1614.